Estimation of Soft Tissue Mechanical Parameters From Robotic Manipulation Data

Pasu Boonvisut, *Student Member, IEEE*, and M. Cenk Çavuşoğlu, *Senior Member, IEEE*

***Abstract*—Robotic motion planning algorithms used for task automation in robotic surgical systems rely on the availability of accurate models of target soft tissue's deformation. Relying on generic tissue parameters in constructing the tissue deformation models is problematic because biological tissues are known to have very large (inter- and intrasubject) variability. *A priori* mechanical characterization (e.g., uniaxial bench test) of the target tissues before a surgical procedure is also not usually practical. In this paper, a method for estimating mechanical parameters of soft tissue from sensory data collected during robotic surgical manipulation is presented. The method uses force data collected from a multiaxial force sensor mounted on the robotic manipulator, and tissue deformation data collected from a stereo camera system. The tissue parameters are then estimated using an inverse finite element method. The effects of measurement and modeling uncertainties on the proposed method are analyzed in simulation. The results of experimental evaluation of the method are also presented.**

***Index Terms*—Biological materials, biological tissues, elasticity, finite element methods, imaging phantoms, manipulators, material properties, materials testing, medical robotics, surgery.**

I. Introduction

ROBOTIC motion planning algorithms being developed to enable robotic surgical assistants (RSAs) to perform certain surgical tasks autonomously while minimizing the damage to the tissue and errors in the operation rely on availability of accurate models of target tissues' deformation. As biological tissues are known to have very large inter- and intrasubject variability, the construction of tissue deformation models using generic tissue parameters is not desirable. However, *a priori* mechanical characterization of the target tissues before a surgical procedure is also not practical. In this paper, a method for estimating the mechanical parameters of manipulated soft tissue from sensory data collected during robotic surgical manipulation is presented. The proposed method does not rely on specialized equipment, sensors, or characterization procedures. Instead, the method uses data collected during typical surgical manipulations, such as, grabbing and retracting the tissue, from a force sensor mounted on the robotic manipulator and a stereo camera system to estimate the tissue parameters. Specifically, the method uses an inverse finite element method (FEM) to estimate the parameters of a nonlinear hyperelastic material model so as to match the estimated tissue response to measured data (see Section III). Several challenge scenarios were simulated to explore the sensitivity of the iterative inverse finite element scheme and the objective function based on uncertainties resulting from RSAs' sensing (see Section IV). Results from experimental evaluation and validation of the method are also presented (see Section V).

Manuscript received December 29, 2011; revised May 13, 2012; accepted July 2, 2012. Recommended by Technical Editor J. Ueda. This work was supported in part by the National Science Foundation under Grant CISE IIS-0805495, Grant IIS-0905344, and Grant CNS-1035602, and in part by the National Institutes of Health under Grant R21 HL096941. This paper was presented in part by the 2012 IEEE International Conference on Robotics and Automation, St. Paul, MN, May 14–18.

The authors are with the Department of Electrical Engineering and Computer Science, Case Western Reserve University, Cleveland, OH 44106 USA (e-mail: bpasu@case.edu; cavusoglu@case.edu).

Color versions of one or more of the figures in this paper are available online at http://ieeexplore.ieee.org.

Digital Object Identifier 10.1109/TMECH.2012.2209673

II. Background

Research on motion planning algorithms for robotic manipulators has traditionally concentrated on manipulation of rigid objects. Recently, however, motion planning algorithms for the manipulation of deformable objects have started to receive attention in the literature (e.g., [2]–[9]).

The robotic motion planning algorithms for the manipulation of deformable objects use models of tissue deformation to estimate the behavior of the object under constraints resulting from the manipulation. Nonlinear finite element models based on continuum mechanics are widely used in many surgery simulations (e.g., [10]–[12]) to estimate large deformations accurately. In general, FEM give higher accuracy at the cost of increased computation. To avoid the computational costs of complex nonlinear FEM, Müller *et al*. [13] proposed a linear FEM with corotational support to improve the simulation accuracy under large deformations. However, nonlinear FEM are preferred when accurate outcomes are needed to perform in surgical simulation [11], [12].

Different tissue models have been used to characterize the hyperelastic deformable object behavior, such as St. Venant–Kirchhoff [14], Veronda–Westmann [11], [12], [15], [16], Arruda–Boyce [17], Neo–Hookean [11], [12], etc.

Traditionally, the parameter sets of different models are examined by performing uniaxial tests. Researchers find the set of parameters that match stress–strain relationship from experiments according to their strain energy model [15]. Recently, iterative parameter identification using inverse finite element analysis has been proposed to determine the set of parameters. Mehrabian and Samani [16] estimated the set of parameters for tissue modeled using the Veronda–Westmann model by performing uniaxial compression testing on polyvinyl alcohol phantom. Sangpradit *et al*. [17] identified the parameters of the Arruda–Boyce model by using wheeled probe indentation on a General Electric RTV6166 silicone phantom.

One of the differences between this study and the earlier studies in the literature is that the parameter estimation scheme presented here does not require any specialized apparatus (such as those used by [18]–[20]), motions, or procedures (such as the performance of a uniaxial loading test [16]).

Most parameter estimation studies have been focused on simple motions such as indentations [17], [21]–[24] and geometrical tension, compression, and shear test [25], [26]. To the best of authors' knowledge, there is a lack of published results for more complicated motions.

Instead, the proposed estimation scheme uses data collected during typical surgical manipulation motions of the manipulator (such as during retraction of the tissue by a gripper). Also, in this study, the deformations of the object surface at multiple points were used in the estimation (similar to [25] which used movements of multiple points inside the tissue as observed through magnetic resonance imaging and which fitted nonlinear material to measured force-displacement samples [22]), unlike earlier studies in the literature that rely on collocated force-displacement measurements (e.g., [17], [27]).

III. Parameter Estimation Scheme

The inputs to the parameter estimation algorithm are the initial geometry of the deformable object (obtained from preoperative medical imaging), the motion of the robotic end-effector grabbing the tissue (given by the joint sensors and kinematics of the robotic manipulator), the tissue interaction forces measured at the robotic end-effector (measured by a six-axis force/torque sensor mounted on the manipulator), and the motions of a set of fiducials on the surface of the deformable object (measured by a stereo camera system). The robotic end-effector motions, tissue interaction forces, and the motion of the fiducials are assumed to be synchronously recorded trajectories.

A. Algorithm

The operation of the parameter estimation algorithm is summarized in Figs. 1 and 2. The algorithm starts with an initial estimate of the mechanical parameters of the target tissue being manipulated (see Fig. 1). Using the estimated mechanical parameters, the simulation loop calculates the deformations of the tissue using a finite element model of the tissue subject to the boundary conditions resulting from specified motion of the robotic end-effector grabbing the tissue. The simulation loop then returns the estimates of the interaction forces and the motions of the fiducials during the manipulation. These estimated interaction forces and fiducial motion trajectories are then compared with the actual trajectories measured by the sensors by using an objective function (described in Section III-B), and checked for convergence. If the objective function has not converged, the estimates of the parameters are updated, and the new parameters are fed back into the simulation loop.

The nonlinear finite element model is employed in the simulation loop (see Fig. 2). The manipulator's initial configuration, the initial tissue geometry and the estimated tissue parameters are used by the nonlinear finite element simulator to solve for the deformation of the tissue in quasi-static state. The deformation

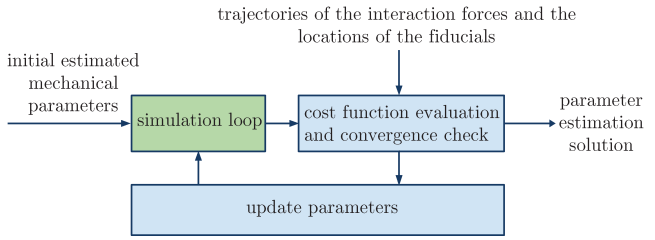

Fig. 1. Flowchart describes the proposed iterative parameter determination scheme.

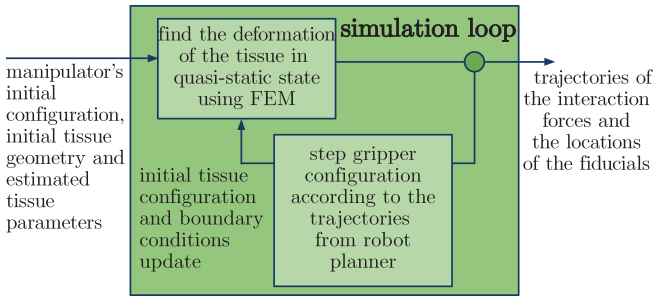

Fig. 2. Diagram illustrates the simulation loop in Fig. 1.

of the tissue in subsequent time steps is then iteratively calculated by using the nonlinear finite element model. At each time step, the configuration of the tissue at the end of the last time step is used as the initial tissue configuration, and the boundary conditions are updated based on the corresponding configuration of the end effector. The trajectories of the interaction forces and the locations of the fiducials on the tissue surface are calculated from the simulation results and are used to evaluate the objective function.

B. Objective Function

Inverse finite element analysis is used to find the set of tissue's parameters that fits the observations. Two different sets of observations are collected from the sensory system. The first set of observations is the interaction forces between the end effector and tissue during the surgical manipulation. The second set of observations is the trajectories of the points of interest fiducials identified on the surface of the tissue. The objective function then has two terms. The first term is a position sensitive term (similar to [22]) and the second term is a force sensitive term. The objective function is then defined as

$$J(\phi) = \sum_{i=1}^{N} \|\boldsymbol{x}_s(\phi, i) - \boldsymbol{x}_o(t_i)\|^2 + \mathscr{C}\|\boldsymbol{f}_s(\phi, i) - \boldsymbol{f}_o(t_i)\|^2 \tag{1}$$

where the subscripts s and o denote, respectively, the simulation and observed outputs, $\boldsymbol{f}$ is the vector representing the forces exerted on the RSA's gripper, and $\boldsymbol{x}$ is the vector representing the trajectories of the points of interest's positions, $\mathscr{C}$ is the scaling factor used to match the scales of the force and position variables, $i = 1, \ldots, N$ are the time indices, and ϕ is the vector representing the set of parameters that specify the tissue's mechanical properties.

Then, the parameter estimation is the minimization of the objective function $J(\phi)$ over the mechanical parameter ϕ as

$$\underset{\phi}{\text{argmin}}\ J(\phi). \tag{2}$$

If desired, the scaling factor can be biased to favor one of the two terms. However, in this study, instead of using a prescribed set value, the scaling factor is automatically determined for each estimate problem as

$$\mathscr{C}_e = \frac{\max_\phi \sum_{i=1}^{N} \|\boldsymbol{x}_s - \boldsymbol{x}_o\|^2 - \min_\phi \sum_{i=1}^{N} \|\boldsymbol{x}_s - \boldsymbol{x}_o\|^2}{\max_\phi \sum_{i=1}^{N} \|\boldsymbol{f}_s - \boldsymbol{f}_o\|^2 - \min_\phi \sum_{i=1}^{N} \|\boldsymbol{f}_s - \boldsymbol{f}_o\|^2}. \tag{3}$$

This $\mathscr{C}_e$ scales both terms equally in the parameter region of interest. Assuming that the tissue simulations always have errors in the force term, the scaling factor is always well-defined.[1] In (3), both of the $\max$ terms are estimated by sampling the region of interest of the parameters while the $\min$ terms are determined by performing numerical minimizations.

C. Tissue Models

In this study, nonlinear finite element models were used to model the deformation of the soft tissues. Nonlinear finite element model stated here means the strain tensor as well as the stress–strain relationship are nonlinear (i.e., both geometric and material nonlinearities are included). For simplification, the analyses were performed for the quasi-static case, neglecting the inertial and damping effects in the tissue dynamics. This is not a restrictive assumption, since manipulation velocities and bandwidths are small in typical surgical manipulations.

The strain energy density function (SEDF) W is a function that relates the Cauchy–Green deformation tensor C of the material to the strain energy density, and is used to characterize nonlinear stress–strain relationship of isotropic hyperelastic materials. In this study, the Neo–Hookean nonlinear material model was used as the underlying material types. The Neo–Hookean model does not have the element inversion problem [28].

The advantage of using a Neo–Hookean material is that it captures the nonlinear nature of material while its parameters still have good physical interpretation. However, it is important to note that the use of the Neo–Hookean material type is not a requirement to the proposed parameter estimation scheme introduced in Section III-B. Different material types can be substituted without any notable change to the method.

The SEDF and stress tensor of the Neo–Hookean material model are given by

$$W = \frac{1}{2}\left(\mu(i_1 - 3) - \mu \log(i_3) + \lambda(\sqrt{i_3} - 1)^2)\right) \tag{4}$$

and

$$S = \mu I - \mu C^{-1} + \lambda(\sqrt{i_3} - 1)\sqrt{i_3}\, C^{-1} \tag{5}$$

respectively [11], [12].

[1]Here, the tissue simulations are assumed to always have errors. In low error cases (such as, for artificial data), it may be desirable to put an upper bound on the scaling factor.

In here, λ and μ are Lamé's first and second parameters, respectively, which can be calculated from Young's modulus E and Poisson's ratio ν of the material by using the relationship

$$\lambda = \frac{E\nu}{(1+\nu)(1-2\nu)} \tag{6}$$

$$\mu = \frac{E}{2(1+\nu)}. \tag{7}$$

i_n is the invariant of the right Cauchy–Green deformation tensor C where only i_1 and i_3 used here are defined as

$$i_1 = \text{trace}(C) \tag{8}$$

$$i_3 = \det(C). \tag{9}$$

IV. Simulation Based Evaluation of The Proposed Method

A. Simulation Methods

In this section, results of the simulation studies of the proposed method are presented. Several different simulation scenarios were used to validate the proposed scheme, and explore its performance under various types of uncertainties.

A limitation of *in vivo* tissue manipulation is that it is difficult to acquire the true state of the tissue to initialize computations and it has greater uncertainties compared to *ex vivo* tests.

The first simulation scenario assumed that the tissue and manipulation geometries were acquired accurately. The second scenario considered the case when the tissue geometry was not perfectly modeled. The third scenario considered the case when there were uncertainties in positioning of the end effector on the target tissue. The fourth scenario considered uncertainties in the robot's motion. And finally, the fifth scenario considered the case when the robot performs nontrivial manipulations.

In the simulations, a tissue model in the shape of a square patch, shown in Fig. 3, with dimensions of $10\,\text{cm} \times 10\,\text{cm} \times 1$ cm was used. The center of the tissue was $(0.0, 0.0, 0.0)$ in x–y–z coordinates. The end-effector gripper was assumed to grasp a 2 cm $\times$ 2 cm area on the tissue without any slip. This was modeled by anchoring the grabbed part of the tissue rigidly to the gripper by position boundary conditions. The size of the gripper was 2 cm in width and initially at $(0.04, 0.0, 0.0)$ m. The tissue was assumed to be anchored on the left side ($x = -5$ cm) and the gripper retracted the tissue by pulling in the direction of the arrow shown in Fig. 3 ($+x$-direction). The stress and strain of the tissue are assumed to be in the zero state at the beginning of the experiment including the effect of gravity.

The `Salmon` [12] open source finite element modeling and simulation package was used as the underlying FEM simulation engine, after custom modifications. The `Salmon` package offers FEM simulation with geometric and material nonlinearities. The meshing of the geometric models to be used in the FEM simulations was done by TetGen [29].

The SQP algorithm using the quasi-Newton line search, as provided by the MATLAB's fmincon function, was used to find minimum of the objective function.

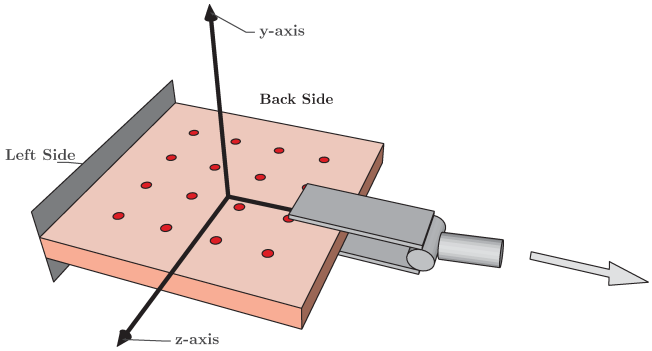

Fig. 3. Setup of the experiment shows the gripper grasping on the right side of tissue and pulling in the direction of the arrow. Sixteen fiducials apart are marked on the tissue. Spacing between rows in both direction is 20 mm.

All experiments were conducted on a 2.93 GHz Intel Core i7 CPU, and 12 GB of RAM. `Salmon` was implemented in the C++ language and MATLAB 2010b was used to implement the optimization scheme.

In the simulation scenarios, all vision and force sensing, i.e., the trajectories of the fiducials and the interaction forces were assumed to have been perfectly measured. The reference values of the sensing data were computed from simulations of a finite element model with a higher density mesh, while the estimation of the set of parameters was performed using a finite element model with a lower density mesh. Specifically, a mesh with 3122 nodes and 13473 elements was used to generate the sensing data, while a mesh with 991 nodes and 3595 elements was used in the estimation process, unless otherwise noted. The reference parameters were 15 kPa and 0.49 for Young's modulus and Poisson's ratio, respectively.

B. Simulation Results

1) Accurate Tissue and Manipulation Geometry Acquisitions: The first set of simulation studies were conducted to validate if the proposed algorithm could accurately identify the tissue parameters under ideal conditions, specifically, when perfect information about the geometry of the specimen and the geometry of manipulation (i.e., motion of the end effector relative to the target tissue) was available. The effect of the density of the finite element model mesh used in the estimation algorithm on the accuracy of the parameter estimation was also evaluated.

In case 1, the tissue model in the estimator was discretized using the higher density mesh (same as the reference). In case 2, the tissue model in the estimator was discretized using the lower density mesh.

The results in Table I show that the proposed method can accurately estimate the tissue parameters under low uncertainty conditions, and the accuracy of the method does not depend heavily on the mesh density (at least, at the range considered here).[2] The parameters estimated in case 2 were reasonably close to the actual values while the complexity is tremendously lower. Therefore, in the subsequent studies (Section IV-B2–IV-B5), the low density mesh was used in estimation while the high-density mesh was used to generate the simulated measurement data.

[2]The nonzero error value in case 1 is due to the finite tolerance value used in numerical minimization.

TABLE I
ESTIMATION RESULTS WHEN ACCURATE TISSUE AND MANIPULATION GEOMETRY MEASUREMENTS ARE AVAILABLE

Case	Case 1	Case 2
Young's Modulus (kPa)	15.18	14.98
Poisson's Ratio	0.4897	0.4849
Iterations (Function Counts)	9(30)	15(46)
Time (s) (prescaling+min)	2452(1469+983)	773 (450+90)
RMSE of		
the fiducial's position (m)	4.32e-6	8.30e-5
the force profile (N)	6.73e-5	2.37e-3

The computation time is represented as total time, which is the sum of the time for prescaling (3), and time for the actual minimization (1). RMSE stands for root mean square error.

TABLE II
EVALUATIONS OF THE METHOD AT DIFFERENT FRACTAL SCALE LEVELS

Fractal Max Height Scale	2%	4%	8%
Young's Modulus (kPa)	17.00	19.40	23.97
Poisson's Ratio	0.4693	0.4654	0.4607
Iter. (Func. Counts)	11(34)	14(42)	4(12)
Time (s) (prescaling+min)	375 (227+148)	897(729+168)	956(785+171)
RMSE of			
the fiducial's position (m)	1.15e-4	1.25e-4	1.36e-4
the force profile (N)	1.69e-3	1.85e-3	2.17e-3

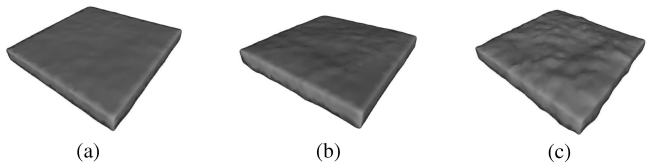

Fig. 4. Unknown parameter tissue with rough surface generated using the ridged multifractal terrain algorithm [30]. (a) Fractal maximum height scale of 2% of the tissue's original thickness. (b) Fractal maximum height scale of 4% of the tissue's original thickness. (c) Fractal maximum height scale of 8% of the tissue's original thickness.

2) Uncertainties in Tissue Geometry: The second set of simulations was conducted to evaluate the effectiveness of the method when the tissue geometry was not perfectly modeled. This was evaluated by using reference meshes which were perturbed from the original shape, while using the original mesh with the smooth surface in the estimation algorithm. The high density mesh was used to generate the test data while the low density mesh (described earlier) was used in parameter estimation.

The rough surfaces in this study were generated using the ridged multifractal terrain algorithm [30] in MeshLab [31] to represent uncertainties in tissue geometry. The results reported in Table II shows the sensitivity of the scheme to the size of the perturbations, at varying 2%, 4%, and 8% of the tissue's original thickness, as can be seen in Fig. 4.

The results demonstrated that the proposed algorithm still handled the problem quite well. Only the Young's modulus was estimated by the method was slightly off when the fractal was higher.

The algorithm that was used to generate fractal in the experiment also grew the tissue. That is the reason why Young's modulus estimated from the scheme increased as the perturbation

TABLE III
EVALUATIONS OF THE SCHEME AT ASSUMING INCORRECT GRASPING POINTS

Standard Deviation	5 mm	10 mm	20 mm
Young's Modulus (kPa)	13.82 ± 12%	12.06 ± 27%	13.33 ± 62%
Poisson's Ratio	0.4677 ± 4%	0.4574 ± 9%	0.3960 ± 28%
Time (s)	966 ± 27%	1445 ± 79%	1023 ± 60%
RMSE of			
the fiducial's position (m)	6.22e-4 ± 65%	1.71e-3 ± 79%	2.94e-3 ± 76%
the force profile (N)	4.22e-2 ± 63%	1.48e-1 ± 63%	1.63e-1 ± 107%

The parameters and other values are the results from 20 random experiments.

TABLE IV
RESULTS WHEN THE GRIPPER POSITION CONTROL SIGNAL WAS CORRUPTED WITH DIFFERENT NOISE LEVELS

Standard Deviation	10%	25%	50%
Young's Modulus (kPa)	14.65 ± 2%	13.88 ± 8%	13.41 ± 19%
Poisson's Ratio	0.4852 ± 2%	0.4733 ± 6%	0.4508 ± 13%
Time (s)	1174 ± 23%	1510 ± 36%	1190 ± 45%
RMSE of			
the fiducial's position (m)	4.14e-4 ± 30%	1.01e-3 ± 29%	2.42e-3 ± 37%
the force profile (N)	3.05e-2 ± 44%	7.66e-2 ± 34%	1.83e-1 ± 66%

The parameters and other values are the results from 20 random experiments.

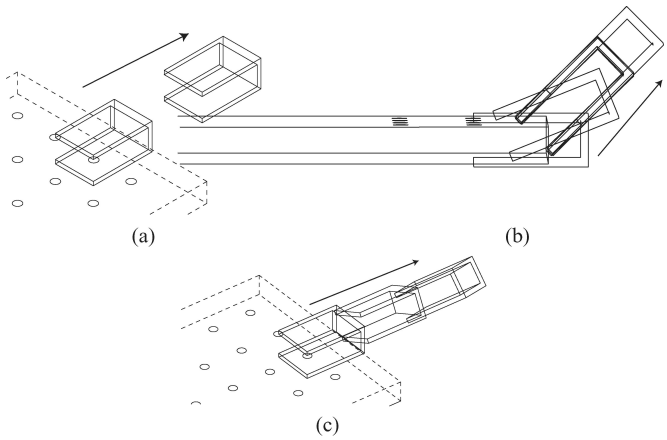

Fig. 5. Different types of complex end-effector motion used to evaluate the parameter estimation in Section IV-B5. (a) "Pull." (b) "Gradual Tangent Pull." (c) "Twist and Pull."

level increased. It is difficult to model the tissue geometry perfectly in simulation; however, the algorithm is robust to small variation shown earlier.

3) Uncertainties in the Position of the Robot's Target: The third set of simulations was conducted to evaluate the effectiveness of the method when there were uncertainties in the positioning of the end effector on the target tissue.

The simulations were done by randomly changing the center of the robot's target (the grasping point) with standard deviation of 5, 10, and 20 mm (see Table III).

The algorithm results are acceptable as shown here.

4) Uncertainties from the Robot's Motion: This set of simulations was conducted to evaluate the effectiveness of the method when there were uncertainties in robot motions. The additive Gaussian noise was generated to study the effect of uncertainties at 10%, 20%, and 50% noise levels (standard deviation of the Gaussian noise as a percent of the magnitude of the position control signal). The results are shown in Table IV.

TABLE V
PARAMETER ESTIMATION UNDER COMPLEX MOTIONS

Motion Types	"Gradual Tangent Pull"	"Twist and Pull'
Young's Modulus (kPa)	15.09	15.06
Poisson's Ratio	0.4720	0.4762
Time (s)	3057(2215+843)	1604(1014+590)
Iter. (Func. Counts)	8(29)	17(51)
RMSE of		
the fiducial's position (m)	2.17e-4	1.68e-4
the force profile (N)	2.06e-2	9.99e-3

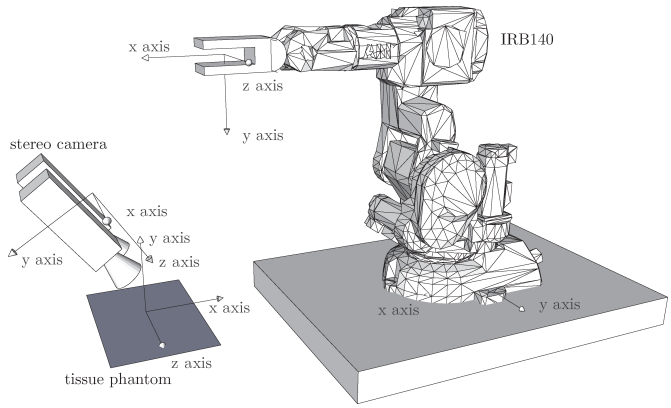

Fig. 6. Setup of the experiments with the ABB IRB 140.

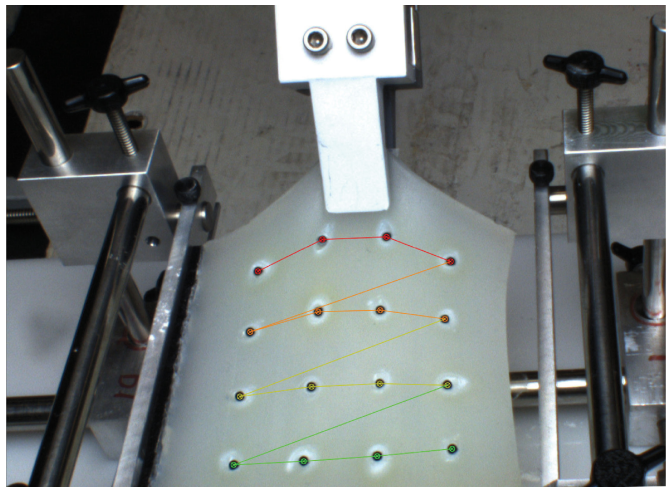

Fig. 7. Robot performing "Gradual Tangent Pull" to retract the Ecoflex 0030 tissue with mixture ratio 1:1:2 anchored two adjacent sides (on the left and at the bottom from the figure) as seen from the right camera.

Noise from the control signal appears not to cause a significant effect on the parameter estimation if the noise level is not extremely high.

5) Parameter Estimation Under Complex Motions: The merit of this multiaxial estimation framework over uniaxial estimation is the ability to estimate the tissue parameters under

TABLE VI
PARAMETER VALUES ESTIMATED BY PERFORMING DIFFERENT ROBOT MANIPULATIONS FOR DIFFERENT TISSUE PHANTOM MATERIALS WHEN ONE SIDE OF THE PHANTOM ARE CONSTRAINED

Motion Types	Pull			Gradual Tangent Pull			Twist and Pull		
Material Types (A:B:T)	1:1:0	1:1:1	1:1:2	1:1:0	1:1:1	1:1:2	1:1:0	1:1:1	1:1:2
Young's Modulus (Pa)	26450	10090	3860	26360	10310	4000	27060	10570	3870
Poisson's Ratio	0.304	0.3134	0.1683	0.2787	0.3394	0.3725	0.3465	0.3504	0.18112
Time (s) (prescaling+min)	892	418	570	1230	683	1174	804	348	2441
Iter. (Func. Counts)	11(36)	9(27)	4(21)	9(27)	9(28)	9(33)	4(12)	8(24)	14(179)

TABLE VII
PARAMETER VALUES ESTIMATED BY PERFORMING DIFFERENT ROBOT MANIPULATIONS FOR DIFFERENT TISSUE PHANTOM MATERIALS WHEN TWO ADJACENT SIDES OF THE PHANTOM ARE CONSTRAINED

Motion Types	Pull			Gradual Tangent Pull			Twist and Pull		
Material Types (A:B:T)	1:1:0	1:1:1	1:1:2	1:1:0	1:1:1	1:1:2	1:1:0	1:1:1	1:1:2
Young's Modulus (Pa)	25230	8620	4070	25250	7770	4130	24960	8660	4480
Poisson's Ratio	0.3984	0.3324	0.3984	0.3416	0.3026	0.3793	0.4157	0.2602	0.1608
Time (s) (prescaling+min)	728	1100	421	1514	1804	988	969	1840	654
Iter. (Func. Counts)	10(35)	9(27)	10(45)	20(76)	8(24)	9(30)	9(29)	25(202)	9(74)

complex surgical manipulations. This set of simulations was conducted to evaluate the effectiveness of the method when the robot had nontrivial motions during a surgical manipulation. Fig. 5 shows the two more different motions used in the simulations. In the first test motion, the gripper horizontally pulled the tissue by simultaneously rotating the gripper. And in the second case, the gripper pulled the tissue horizontally in the tissue plane while rotating the tissue to twist it.

The results in Table V show that the method can still estimate the parameters with good accuracy under such complex motions.

V. EXPERIMENTAL VALIDATION OF THE PROPOSED METHOD

A. Experimental Method

In order to validate the proposed method, hardware experiments were conducted. In the experiments, we used a soft tissue phantom created using Ecoflex 0030, a two-part silicone rubber with Silicone Thinner (nonreactive silicone fluid), from Smooth–On Inc., which was used in [32]. The silicone phantoms with three different consistencies of Silicone Thinner were used in order to cover a wide range of parameter values. ABB IRB 140, a 6-DOF robot equipped with the Gamma SI-130-10 force sensor (ATI Industrial Automation, Inc., Apex, NC) with resolution of 1/20 N was used to collect the manipulation trajectories and force sensing data. The repeatability of the robot is 0.03 mm. The setup of the experiments is shown in Fig. 6.

The tissue phantoms used in the experiments were similar in shape and size to the models used in the simulation studies described in Section IV-A. Specifically, the tissue phantoms were square in shape, with dimensions of $10\,\text{cm} \times 10\,\text{cm} \times 1\,\text{cm}$. The tissue phantoms were placed horizontally while being grabbed and retracted by a gripper toward right. We considered two cases where the phantoms were anchored to a wall on one side (left) and two adjacent sides (left and back). The retraction actions were achieved by moving the gripper in 1–2 mm increments, toward right, producing about 10% elongation of the tissue phantom as shown in Fig. 5. The "Pull" trajectory was performed in 10 steps with 2 mm increments; the "Gradual Tangent Pull" trajectory was performed in 20 steps with $\sim$1 mm increments; and the "Twist and Pull" trajectory was performed in 10 steps with $\sim$2 mm increments. Sixteen artificial fiducials were marked on the top surface of the tissue and were tracked by a calibrated stereo camera pair to measure their deformations during retraction.

The silicone surface was labeled with rubber beads 1 mm in diameter which were used as the fiducials. The stereo vision system employed two of identical FL2G-13S2C 1.2MP cameras (Point Gray Research, Richmond, BC, Canada). The cameras were placed at a distance of 30 cm. The cameras were programmed using the Flycapture library (Point Gray Research, Richmond, BC, Canada) and OpenCV. Once the fiducials were detected, each individual fiducial location was calculated by distinguishing each fiducial in the image. After the fiducials were detected in the stereo image pair (see Fig. 7), the actual locations of the fiducials were triangulated using the camera calibration information.

One important concern regarding experimental validation of the proposed methods is the availability of baseline material parameters (Young's modulus and Poisson's ratio) for the silicone rubber used in constructing the phantoms. The only material property that the authors could identify in the literature for Ecoflex 0030 was for the 1:1:0 mixture proportions [32].[3] Hollenstein has reported a Young's modulus of 29.5 kPa, while a Poission ratio of 0.5 was assumed. In order

[3]To the best of our effort, these were the only parameter values that we were able to find in the literature for the Ecoflex silicone.

TABLE VIII

ACTUAL (SHOWN IN SOLID) AND THE PREDICTED (SHOWN IN DASH) INTERACTION FORCE PROFILES IN TISSUE COORDINATE FRAME (X-, Y-, AND Z-AXES ARE SHOWN IN BLUE, GREEN, AND RED, RESPECTIVELY) AND THE ACTUAL (BLACK/DARK) AND PREDICTED (RED/BRIGHT) TRAJECTORIES OF THE FIDUCIAL MARKERS WHEN TWO ADJACENT SIDES OF THE PHANTOM ARE CONSTRAINED

Ecoflex 0030 Mixing Ratio		
1:1:0	1:1:1	1:1:2
Pull		
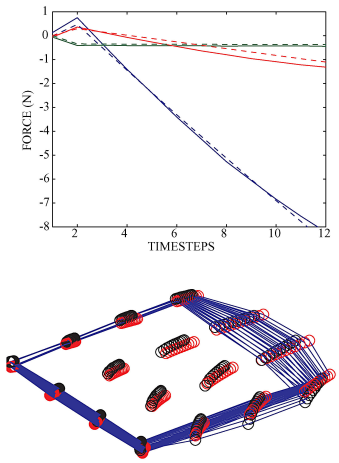	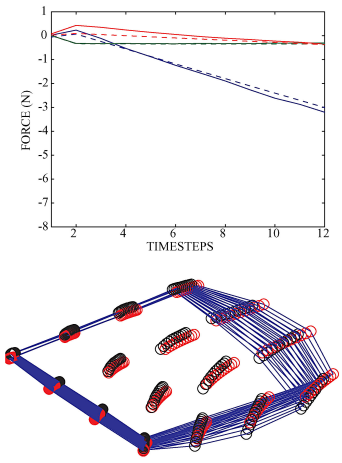	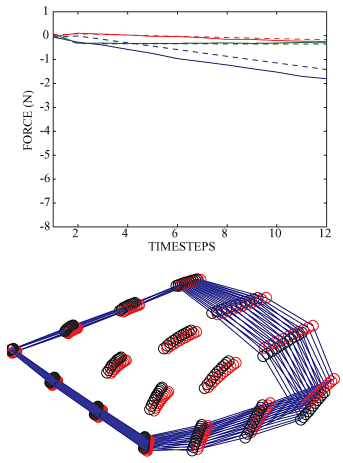
Gradual Tangent Pull		
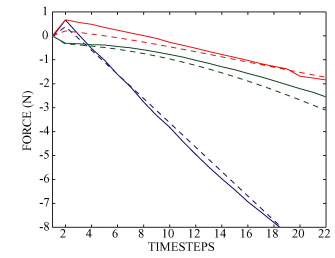	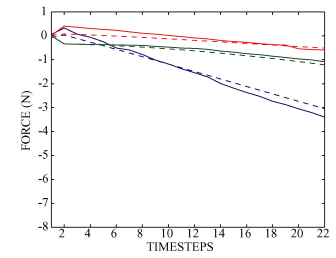	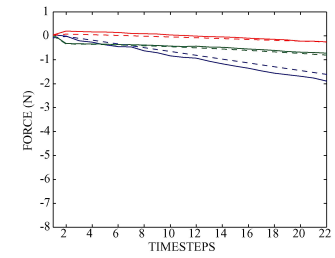
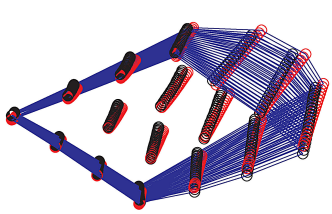	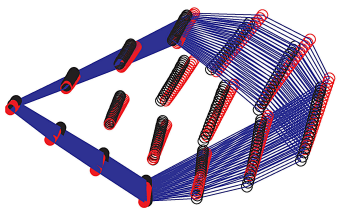	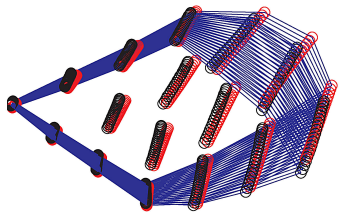
Twist and Pull		
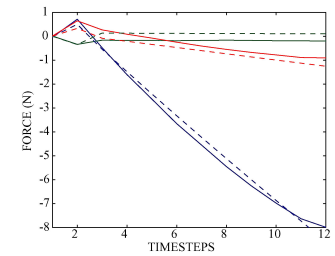	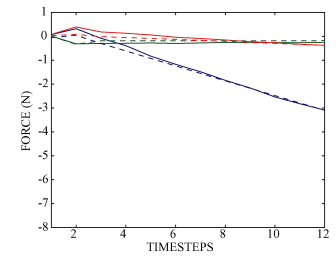	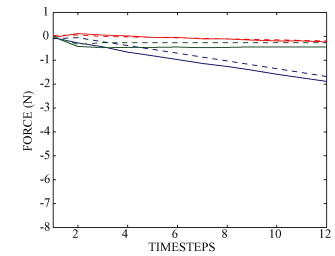
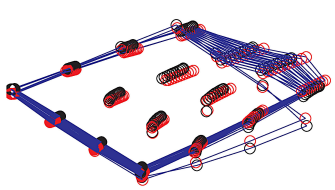	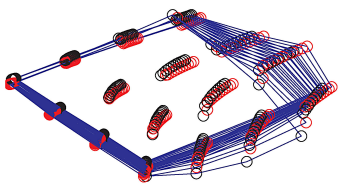	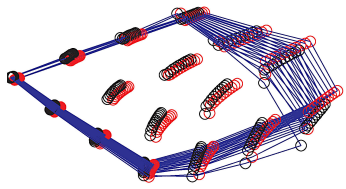

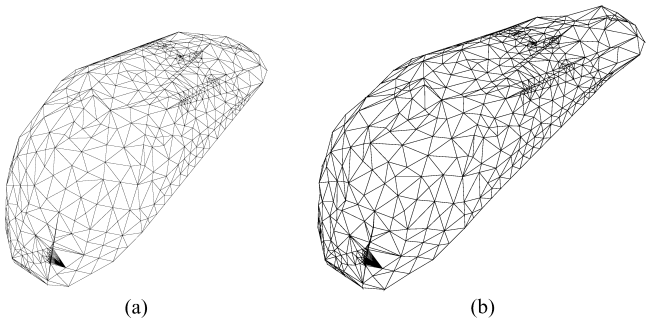

Fig. 8. (a) Undeformed and (b) deformed liver models. The model was anchored on the left side while being grasped and pulled on the right side.

to obtain the necessary baseline material property data, we conducted standard uniaxial loading tests. Specifically, hourglass-shaped specimens of the silicone rubber material were constructed and they were tested on a universal testing machine (Instron 1026). Young's moduli estimated by the uniaxial testing of Ecoflex 0030 for the mixture proportions 1:1:0, 1:1:1, and 1:1:2 were, respectively, 36.21 ± 2.62 kPa, 10.91 ± 1.54 kPa, and 5.29 ± 1.92 kPa. A Poisson's ratio of 0.5 was assumed.

The stress and strain of the tissue are assumed to be in zero state at the beginning of the experiment. Here, we do not neglect the effect of gravity.

B. Experimental Results

Different tissue consistencies were obtained by using different silicone rubber and silicone thinner proportions during the preparation of the phantoms. The parameter estimates for the three different tissue phantoms are reported in Tables VI and VII. The values estimated here using the proposed method are very close to the reported parameter values for the Ecoflex 0030 mixture ratio of 1:1:0 from the literature [32] and the results from the universal testing machine for the mixture ratio of 1:1:1 and 1:1:2 in Section V-A. Note that, using the proposed method, we estimated both Young's moduli and Poisson's ratios simultaneously instead of assuming Poisson's ratios to be 0.5. Estimating the parameters simultaneously helps us to have a better prediction in geometric configurations of the tissue.

In order to save space, the figures showing the trajectories of the fiducials and the force profiles for the cases in Table VI are omitted. The trajectories of fiducials and the force profiles for the cases in Table VII are shown in Table VIII. The figures in Table VIII show that the fiducial trajectories and force profiles start to deviate from the actual trajectories for large deformations, even though there is a good agreement between the estimated and actual trajectories for relatively smaller deformations. Note that in constrast to some literatures (for example [32]), Poisson's ratio was actually estimated from the algorithm instead of assuming the value to 0.5. Doing this way, we found that the estimated tissue responses and the real physical data are in a better agreement than the response assuming Poisson's ratio to such a number. We believe this deviations are due to the material type used, as Neo–Hookean might not be the best choice for highly nonlinear materials.

VI. Example: Parameter Estimation With More Complex Object Geometries

The parameter estimation examples presented earlier in this paper primarily used regular shapes for object geometry in order to allow easier interpretation of the results. The proposed method is also applicable to more complex object shape, such as those that would be encountered in practical applications.

In order to evaluate the performance of the proposed method for nonregular object geometries, a simulation study was conducted. In this simulation, a tissue model in the shape of liver, shown in Fig. 8(a), was used [33]. The liver model was assumed to be anchored on one side while being grasped and pulled on the opposite side, as shown in Fig. 8(b). The reference deformation and force trajectories were generated using a 2803 node and 13737 element mesh model, using Young's modulus value of 15 kPa and Poisson's ratio of 0.35. The parameter estimation was performed using a 1033 node and 4095 element mesh model.

The parameters estimated using the presented algorithm were 13.36 kPa and 0.30 for Young's modulus and Poisson's ratio, respectively. The mean error of fiducial trajectories estimated from the the estimated parameters was less than 0.9 mm and was less than 0.46% of the total trajectory. The maximum force error was 1.5 N and that was 2.2% of the total force. It is demonstrative that the algorithm may also be used for parameter estimation for nonregular object shapes.

VII. Discussion and Conclusion

This paper presented a new inverse nonlinear finite element-based scheme to estimate the mechanical parameters of soft tissues using data collected during regular manipulation of the tissue in robotic surgery. The method uses a hyperelastic material model for the tissue. Several challenge scenarios and different types of complex motions were considered to test the sensitivity of the proposed scheme. Results of the method are evaluated and validated experimentally as well. The simulation and experimental results indicated that the proposed scheme is effective in estimating the parameters in general.

Typical surgical manipulation motions are relatively slow. Therefore, the tissue deformations and interactions forces were approximated as quasi-static, ignoring the viscous and inertial effects.

It is important to note that the proposed approach assumed homogeneous material. Although the proposed approach could be applicable for moderate nonhomogeneities, the identification of a very detailed inhomogeneous model (e.g., objects with lots of embedded fine structures), where identifications of the material parameters of the embedded fine structures are sought, would require a more data-rich method, such as magnetic resonance elastography [25], [34]–[37] and ultrasound elastometry [38].

Uncertainty in boundary conditions, including complex boundary conditions, such as frictional sliding contact resulting from an object sliding over another object, has been considered

in this study to some extent. The aspect of the problem needs to be further studied.

It is also important to note that the choice of the Neo–Hookean material type is not fundamental to the proposed method. The same overall tissue parameter estimation method can also be applied by using different underlying material types. However, whether the sufficient accuracy is obtainable or not for different material types needs to be verified. A detailed analysis and comparison of different material types is outside the scope of this paper.

ACKNOWLEDGMENT

The authors would like to thank Prof. J. Lewandowski and Prof. W. Newman for their valuable suggestions and for allowing us to use the facilities to perform the experiments. They would also like thank R. Jackson and C. Balin for their stereo-vision implementations.

REFERENCES

[1] P. Boonvisut, R. Jackson, and M. C. Çavuşoğlu, "Estimation of soft tissue mechanical parameters from robotic manipulation data," in *Proc. Int. Conf. Robot. Autom.*, May 2012, pp. 4667–4674.

[2] S. Hirai, T. Tsuboi, and T. Wada, "Robust grasping manipulation of deformable objects," in *Proc. IEEE Int. Symp. Assembly Task Planning*, 2001, pp. 411–416.

[3] K. Gopalakrishnan and K. Goldberg, "D-Space and deform closure grasps of deformable parts," *Int. J. Robot. Res.*, vol. 24, no. 11, pp. 899–910, 2005.

[4] M. Moll and L. E. Kavraki, "Path planning for deformable linear objects," *IEEE Trans. Robot.*, vol. 22, no. 4, pp. 625–636, Aug. 2006.

[5] M. Saha and P. Isto, "Motion planning for robotic manipulation of deformable linear objects," in *Proc. IEEE Int. Conf. Robot. Autom.*, 2006, pp. 2478–2484.

[6] M. Saha and P. Isto, "Manipulation planning for deformable linear objects," *IEEE Trans. Robot.*, vol. 23, no. 6, pp. 1141–1150, Dec. 2007.

[7] R. Alterovitz, M. Branicky, and K. Goldberg, "Motion planning under uncertainty for image-guided medical needle steering," *Int. J. Robot. Res.*, vol. 27, no. 11–12, pp. 1361–1374, Nov. 2008.

[8] R. Alterovitz, K. Y. Goldberg, J. Pouliot, and I. C. Hsu, "Sensorless motion planning for medical needle insertion in deformable tissues," *IEEE Trans. Inf. Technol. Biomed.*, vol. 13, no. 2, pp. 217–225, Mar. 2009.

[9] R. Jansen, K. Hauser, N. Chentanez, F. van der Stappen, and K. Goldberg, "Surgical retraction of non-uniform deformable layers of tissue: 2D robot grasping and path planning," in *Proc. IEEE Int. Conf. Intell. Robots Syst.*, St Louis, MO, Oct. 2009, pp. 4092–4097.

[10] M. Bro-nielsen, "Finite element modeling in surgery simulation," *Proc. IEEE: Special Issue on Surgery Simulation*, vol. 86, pp. 490–503, 1998.

[11] X. Wu, "Design of an interactive nonlinear finite element based deformable object simulator," Ph.D. dissertation, Dept. Mech. Eng., Univ. California Berkeley, Berkeley, 2002.

[12] H.-W. Nienhuys, "Cutting in deformable objects," Ph.D. dissertation, Inst. Inf. Comput. Sci., Utrecht Univ., Utrecht, The Netherlands, 2003.

[13] M. Müller, J. Dorsey, L. McMillan, R. Jagnow, and B. Cutler, *Stable Real-Time deformations.* New York: ACM Press, 2002, pp. 49–54.

[14] J. Barbič and D. L. James, "Real-time subspace integration for St. Venant-Kirchhoff deformable models," *ACM Trans. Graph. (SIGGRAPH)*, vol. 24, no. 3, pp. 982–990, Aug. 2005.

[15] D. R. Veronda and R. A. Westmann, "Mechanical characterization of skin—Finite deformations," *J. Biomech.*, vol. 3, no. 1, pp. 111–124, Jan. 1970.

[16] H. Mehrabian and A. Samani, "Constrained hyperelastic parameters reconstruction of PVA (Polyvinyl Alcohol) phantom undergoing large deformation," in *Medical Imaging 2009: Visualization, Image-Guided Procedures, and Modeling*, M. I. Miga and K. H. Wong, Eds., vol. 7261. Bellingham, WA: SPIE, 2009, no. 1.

[17] K. Sangpradit, H. Liu, L. D. Seneviratne, and K. Althoefer, "Tissue identification using inverse finite element analysis of rolling indentation," in *Proc. IEEE Int. Conf. Robot. Autom.*, May 2009, pp. 1250–1255.

[18] M. P. Ottensmeyer, "Minimally invasive instrument for *in vivo* measurement of solid organ mechanical impedance," Ph.D. dissertation, Dept. Mech. Eng., Massachusetts Inst. Technol., Cambridge, MA, 2001.

[19] M. Kauer, V. Vuskovic, J. Dual, G. Szekely, and M. Bajka, "Inverse finite element characterization of soft tissues," *Med. Image Anal.*, vol. 6, no. 3, pp. 275–287, 2002.

[20] I. Brouwer, J. Ustin, L. Bentley, A. Sherman, N. Dhruv, and F. Tendick, "Measuring *in vivo* animal soft tissue properties for haptic modeling in surgical simulation," *Stud. Health Technol. Inf.*, vol. 81, pp. 69–74, 2001.

[21] J. Lang, D. K. Pai, and R. J. Woodham, "Acquisition of elastic models for interactive simulation," *Int. J. Robot. Res.*, vol. 21, no. 8, pp. 713–733, Aug. 2002.

[22] B. Bickel, M. Bächer, M. A. Otaduy, W. Matusik, H. Pfister, and M. Gross, "Capture and modeling of non-linear heterogeneous soft tissue," in *Proc. ACM SIGGRAPH*, 2009, pp. 1–9.

[23] P. Fong, "Sensing, acquisition, and interactive playback of data-based models for elastic deformable objects," *Int. J. Robot. Res.*, vol. 28, no. 5, pp. 630–655, May 2009.

[24] B. Frank, R. Schmedding, C. Stachniss, M. Teschner, and W. Burgard. (2010, Oct.). "Learning the elasticity parameters of deformable objects with a manipulation robot," pp. 1877–1883, [Online]. Available: http://dx.doi.org/10.1109/IROS.2010.5653949

[25] A. E. Kerdok, S. M. Cotin, M. P. Ottensmeyer, A. M. Galea, R. D. Howe, and S. L. Dawson, "Truth cube: Establishing physical standards for soft tissue simulation," *Med. Image Anal.*, vol. 7, no. 3, pp. 283–291, Sep. 2003.

[26] Z. Gao, K. Lister, and J. Desai, "Constitutive modeling of liver tissue: Experiment and theory," *Ann. Biomed. Eng.*, vol. 38, no. 2, pp. 505–516, 2010.

[27] D. d'Aulignac, M. C. Çavuşoglu, and C. Laugier, "Modeling the dynamics of the human thigh for a realistic echographic simulator with force feedback," in *MICCAI '99: Proceedings of the Second International Conference on Medical Image Computing and Computer-Assisted Intervention*. London, U.K.: Springer-Verlag, 1999, pp. 1191–1198.

[28] G. Irving, J. Teran, and R. Fedkiw, "Invertible finite elements for robust simulation of large deformation," in *SCA '04: Proceedings of the 2004 ACM SIGGRAPH/Eurographics Symposium on Computer Animation*. Aire-la-Ville, Switzerland: Eurographics Association, 2004, pp. 131–140.

[29] H. Si, "Tetgen: A quality tetrahedral mesh generator and a 3D delaunay triangulator," [Online]. Available: http://tetgen.berlios.de/.

[30] D. S. Ebert, F. K. Musgrave, D. Peachey, K. Perlin, and S. Worley, *Texturing and Modeling, Third Edition: A Procedural Approach (The Morgan Kaufmann Series in Computer Graphics)*, 3rd ed. San Mateo, CA: Morgan Kaufmann, Dec. 2002.

[31] P. Cignoni, M. Callieri, M. Corsini, M. Dellepiane, F. Ganovelli, and G. Ranzuglia. (2008). "MeshLab: An Open-Source mesh processing tool," pp. 129–136, [Online]. Available: http://vcg.isti.cnr.it/Publications/2008/CCCDGR08

[32] M. Hollenstein, "Mechanical characterization of soft materials: Comparison between different experiments on synthetic specimens," Master's thesis, Inst. Mech. Syst. Dept. Mech. Process Eng., ETH Zurich, Eidgenössische Technische Hochschule Zurich, Zurich, Switzerland, 2008.

[33] J. Allard, S. Cotin, F. Faure, P.-J. J. Bensoussan, F. Poyer, C. Duriez, H. Delingette, and L. Grisoni, "SOFA—An open source framework for medical simulation," *Stud. Health Technol. Informat.*, vol. 125, pp. 13–18, 2007.

[34] X. Shi, R. W. Martin, D. Rouseff, S. Vaezy, and L. A. Crum, "Detection of high-intensity focused ultrasound liver lesions using dynamic elastometry," *Ultrason. Imag.*, vol. 21, no. 2, pp. 107–126, Apr. 1999.

[35] R. Sinkus, J. Lorenzen, D. Schrader, M. Lorenzen, M. Dargatz, and D. Holz, "High-resolution tensor MR elastography for breast tumour detection," *Phys. Med. Biol.*, vol. 45, no. 6, pp. 1649–1664, Jun. 2000.

[36] S. K. Venkatesh, M. Yin, J. F. Glockner, N. Takahashi, P. A. Araoz, J. A. Talwalkar, and R. L. Ehman, "MR elastography of liver tumors: Preliminary results," *AJR. Amer. J. Roentgenol*, vol. 190, no. 6, pp. 1534–1540.

[37] S. F. Bensamoun, L. Wang, L. Robert, F. Charleux, J.-P. P. Latrive, and M.-C. Ho Ba Tho, "Measurement of liver stiffness with two imaging techniques: Magnetic resonance elastography and ultrasound elastometry," *J. Magn. Reson. Imag.*, vol. 28, no. 5, pp. 1287–1292, Nov. 2008.

[38] E. Turgay, S. Salcudean, and R. Rohling, "Identifying the mechanical properties of tissue by ultrasound strain imaging," *Ultrasound Med. Biol.*, vol. 32, no. 2, pp. 221–235, Feb. 2006.

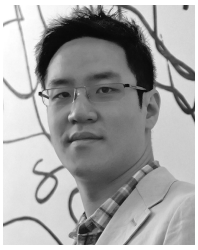

Pasu Boonvisut (S'12) received the B.Eng. and M.Eng. degrees in electrical engineering from Chulalongkorn University, Bangkok, Thailand, in 2005 and 2007, respectively. He is currently working toward the Ph.D. degree at Case Western Reserve University, Cleveland, OH.

His research interests include medical robotics and digital signal processing.

M. Cenk Çavuşoğlu (S'93–M'01–SM'06) received the B.S. degree in electrical and electronic engineering from Middle East Technical University, Ankara, Turkey, in 1995, and the M.S. and Ph.D. degrees in electrical engineering and computer sciences from the University of California, Berkeley, in 1997 and 2000, respectively.

He is currently an Associate Professor of electrical engineering and computer science at Case Western Reserve University, Cleveland, OH. Previously, he was a Visiting Researcher at the INRIA Rhones-Alpes Research Center, France, in 1998, a Postdoctoral Researcher and Lecturer at the University of California, Berkeley, from 2000 to 2002, and a Visiting Associate Professor at Bilkent University, Ankara, Turkey, from 2009 to 2010. His research involves applications of robotics and control engineering to biomedical and biologically inspired engineered systems. Specifically, his research interests include robotics, systems and control theory, and human–machine interfaces, with emphasis on medical robotics, haptics, virtual environments, surgical simulation, and biosystem modeling and simulation.

Dr. Çavuşoğlu is currently serving as an Associate Editor of the IEEE TRANSACTIONS ON ROBOTICS, and as a Technical Editor of the IEEE/ASME TRANSACTIONS ON MECHATRONICS.

Estimation of Soft Tissue Mechanical Parameters From Robotic Manipulation Data

Pasu Boonvisut, *Student Member, IEEE*, and M. Cenk Çavuşoğlu, *Senior Member, IEEE*

***Abstract*—Robotic motion planning algorithms used for task automation in robotic surgical systems rely on the availability of accurate models of target soft tissue's deformation. Relying on generic tissue parameters in constructing the tissue deformation models is problematic because biological tissues are known to have very large (inter- and intrasubject) variability. *A priori* mechanical characterization (e.g., uniaxial bench test) of the target tissues before a surgical procedure is also not usually practical. In this paper, a method for estimating mechanical parameters of soft tissue from sensory data collected during robotic surgical manipulation is presented. The method uses force data collected from a multiaxial force sensor mounted on the robotic manipulator, and tissue deformation data collected from a stereo camera system. The tissue parameters are then estimated using an inverse finite element method. The effects of measurement and modeling uncertainties on the proposed method are analyzed in simulation. The results of experimental evaluation of the method are also presented.**

***Index Terms*—Biological materials, biological tissues, elasticity, finite element methods, imaging phantoms, manipulators, material properties, materials testing, medical robotics, surgery.**

I. Introduction

ROBOTIC motion planning algorithms being developed to enable robotic surgical assistants (RSAs) to perform certain surgical tasks autonomously while minimizing the damage to the tissue and errors in the operation rely on availability of accurate models of target tissues' deformation. As biological tissues are known to have very large inter- and intrasubject variability, the construction of tissue deformation models using generic tissue parameters is not desirable. However, *a priori* mechanical characterization of the target tissues before a surgical procedure is also not practical. In this paper, a method for estimating the mechanical parameters of manipulated soft tissue from sensory data collected during robotic surgical manipulation is presented. The proposed method does not rely on specialized equipment, sensors, or characterization procedures. Instead, the method uses data collected during typical surgical manipulations, such as, grabbing and retracting the tissue, from a force sensor mounted on the robotic manipulator and a stereo camera system to estimate the tissue parameters. Specifically, the method uses an inverse finite element method (FEM) to estimate the parameters of a nonlinear hyperelastic material model so as to match the estimated tissue response to measured data (see Section III). Several challenge scenarios were simulated to explore the sensitivity of the iterative inverse finite element scheme and the objective function based on uncertainties resulting from RSAs' sensing (see Section IV). Results from experimental evaluation and validation of the method are also presented (see Section V).

Manuscript received December 29, 2011; revised May 13, 2012; accepted July 2, 2012. Recommended by Technical Editor J. Ueda. This work was supported in part by the National Science Foundation under Grant CISE IIS-0805495, Grant IIS-0905344, and Grant CNS-1035602, and in part by the National Institutes of Health under Grant R21 HL096941. This paper was presented in part by the 2012 IEEE International Conference on Robotics and Automation, St. Paul, MN, May 14–18.

The authors are with the Department of Electrical Engineering and Computer Science, Case Western Reserve University, Cleveland, OH 44106 USA (e-mail: bpasu@case.edu; cavusoglu@case.edu).

Color versions of one or more of the figures in this paper are available online at http://ieeexplore.ieee.org.

Digital Object Identifier 10.1109/TMECH.2012.2209673

II. Background

Research on motion planning algorithms for robotic manipulators has traditionally concentrated on manipulation of rigid objects. Recently, however, motion planning algorithms for the manipulation of deformable objects have started to receive attention in the literature (e.g., [2]–[9]).

The robotic motion planning algorithms for the manipulation of deformable objects use models of tissue deformation to estimate the behavior of the object under constraints resulting from the manipulation. Nonlinear finite element models based on continuum mechanics are widely used in many surgery simulations (e.g., [10]–[12]) to estimate large deformations accurately. In general, FEM give higher accuracy at the cost of increased computation. To avoid the computational costs of complex nonlinear FEM, Müller *et al*. [13] proposed a linear FEM with corotational support to improve the simulation accuracy under large deformations. However, nonlinear FEM are preferred when accurate outcomes are needed to perform in surgical simulation [11], [12].

Different tissue models have been used to characterize the hyperelastic deformable object behavior, such as St. Venant–Kirchhoff [14], Veronda–Westmann [11], [12], [15], [16], Arruda–Boyce [17], Neo–Hookean [11], [12], etc.

Traditionally, the parameter sets of different models are examined by performing uniaxial tests. Researchers find the set of parameters that match stress–strain relationship from experiments according to their strain energy model [15]. Recently, iterative parameter identification using inverse finite element analysis has been proposed to determine the set of parameters. Mehrabian and Samani [16] estimated the set of parameters for tissue modeled using the Veronda–Westmann model by performing uniaxial compression testing on polyvinyl alcohol phantom. Sangpradit *et al*. [17] identified the parameters of the Arruda–Boyce model by using wheeled probe indentation on a General Electric RTV6166 silicone phantom.

One of the differences between this study and the earlier studies in the literature is that the parameter estimation scheme presented here does not require any specialized apparatus (such as those used by [18]–[20]), motions, or procedures (such as the performance of a uniaxial loading test [16]).

Most parameter estimation studies have been focused on simple motions such as indentations [17], [21]–[24] and geometrical tension, compression, and shear test [25], [26]. To the best of authors' knowledge, there is a lack of published results for more complicated motions.

Instead, the proposed estimation scheme uses data collected during typical surgical manipulation motions of the manipulator (such as during retraction of the tissue by a gripper). Also, in this study, the deformations of the object surface at multiple points were used in the estimation (similar to [25] which used movements of multiple points inside the tissue as observed through magnetic resonance imaging and which fitted nonlinear material to measured force-displacement samples [22]), unlike earlier studies in the literature that rely on collocated force-displacement measurements (e.g., [17], [27]).

III. Parameter Estimation Scheme

The inputs to the parameter estimation algorithm are the initial geometry of the deformable object (obtained from preoperative medical imaging), the motion of the robotic end-effector grabbing the tissue (given by the joint sensors and kinematics of the robotic manipulator), the tissue interaction forces measured at the robotic end-effector (measured by a six-axis force/torque sensor mounted on the manipulator), and the motions of a set of fiducials on the surface of the deformable object (measured by a stereo camera system). The robotic end-effector motions, tissue interaction forces, and the motion of the fiducials are assumed to be synchronously recorded trajectories.

A. Algorithm

The operation of the parameter estimation algorithm is summarized in Figs. 1 and 2. The algorithm starts with an initial estimate of the mechanical parameters of the target tissue being manipulated (see Fig. 1). Using the estimated mechanical parameters, the simulation loop calculates the deformations of the tissue using a finite element model of the tissue subject to the boundary conditions resulting from specified motion of the robotic end-effector grabbing the tissue. The simulation loop then returns the estimates of the interaction forces and the motions of the fiducials during the manipulation. These estimated interaction forces and fiducial motion trajectories are then compared with the actual trajectories measured by the sensors by using an objective function (described in Section III-B), and checked for convergence. If the objective function has not converged, the estimates of the parameters are updated, and the new parameters are fed back into the simulation loop.

The nonlinear finite element model is employed in the simulation loop (see Fig. 2). The manipulator's initial configuration, the initial tissue geometry and the estimated tissue parameters are used by the nonlinear finite element simulator to solve for the deformation of the tissue in quasi-static state. The deformation

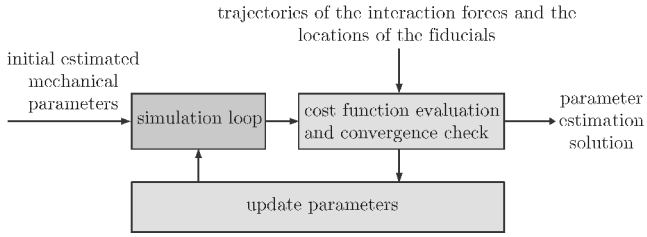

Fig. 1. Flowchart describes the proposed iterative parameter determination scheme.

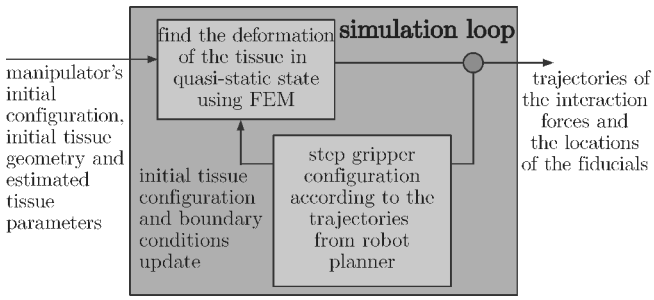

Fig. 2. Diagram illustrates the simulation loop in Fig. 1.

of the tissue in subsequent time steps is then iteratively calculated by using the nonlinear finite element model. At each time step, the configuration of the tissue at the end of the last time step is used as the initial tissue configuration, and the boundary conditions are updated based on the corresponding configuration of the end effector. The trajectories of the interaction forces and the locations of the fiducials on the tissue surface are calculated from the simulation results and are used to evaluate the objective function.

B. Objective Function

Inverse finite element analysis is used to find the set of tissue's parameters that fits the observations. Two different sets of observations are collected from the sensory system. The first set of observations is the interaction forces between the end effector and tissue during the surgical manipulation. The second set of observations is the trajectories of the points of interest fiducials identified on the surface of the tissue. The objective function then has two terms. The first term is a position sensitive term (similar to [22]) and the second term is a force sensitive term. The objective function is then defined as

$$J(\phi) = \sum_{i=1}^{N} \|\boldsymbol{x}_s(\phi, i) - \boldsymbol{x}_o(t_i)\|^2 + \mathscr{C}\|\boldsymbol{f}_s(\phi, i) - \boldsymbol{f}_o(t_i)\|^2 \tag{1}$$

where the subscripts s and o denote, respectively, the simulation and observed outputs, $\boldsymbol{f}$ is the vector representing the forces exerted on the RSA's gripper, and $\boldsymbol{x}$ is the vector representing the trajectories of the points of interest's positions, $\mathscr{C}$ is the scaling factor used to match the scales of the force and position variables, $i = 1, \ldots, N$ are the time indices, and ϕ is the vector representing the set of parameters that specify the tissue's mechanical properties.

Then, the parameter estimation is the minimization of the objective function $J(\phi)$ over the mechanical parameter ϕ as

$$\underset{\phi}{\text{argmin}}\ J(\phi). \tag{2}$$

If desired, the scaling factor can be biased to favor one of the two terms. However, in this study, instead of using a prescribed set value, the scaling factor is automatically determined for each estimate problem as

$$\mathscr{C}_e = \frac{\max_\phi \sum_{i=1}^{N} \|\boldsymbol{x}_s - \boldsymbol{x}_o\|^2 - \min_\phi \sum_{i=1}^{N} \|\boldsymbol{x}_s - \boldsymbol{x}_o\|^2}{\max_\phi \sum_{i=1}^{N} \|\boldsymbol{f}_s - \boldsymbol{f}_o\|^2 - \min_\phi \sum_{i=1}^{N} \|\boldsymbol{f}_s - \boldsymbol{f}_o\|^2}. \tag{3}$$

This $\mathscr{C}_e$ scales both terms equally in the parameter region of interest. Assuming that the tissue simulations always have errors in the force term, the scaling factor is always well-defined.[1] In (3), both of the $\max$ terms are estimated by sampling the region of interest of the parameters while the $\min$ terms are determined by performing numerical minimizations.

C. Tissue Models

In this study, nonlinear finite element models were used to model the deformation of the soft tissues. Nonlinear finite element model stated here means the strain tensor as well as the stress–strain relationship are nonlinear (i.e., both geometric and material nonlinearities are included). For simplification, the analyses were performed for the quasi-static case, neglecting the inertial and damping effects in the tissue dynamics. This is not a restrictive assumption, since manipulation velocities and bandwidths are small in typical surgical manipulations.

The strain energy density function (SEDF) W is a function that relates the Cauchy–Green deformation tensor C of the material to the strain energy density, and is used to characterize nonlinear stress–strain relationship of isotropic hyperelastic materials. In this study, the Neo–Hookean nonlinear material model was used as the underlying material types. The Neo–Hookean model does not have the element inversion problem [28].

The advantage of using a Neo–Hookean material is that it captures the nonlinear nature of material while its parameters still have good physical interpretation. However, it is important to note that the use of the Neo–Hookean material type is not a requirement to the proposed parameter estimation scheme introduced in Section III-B. Different material types can be substituted without any notable change to the method.

The SEDF and stress tensor of the Neo–Hookean material model are given by

$$W = \frac{1}{2}\left(\mu(i_1 - 3) - \mu \log(i_3) + \lambda(\sqrt{i_3} - 1)^2)\right) \tag{4}$$

and

$$S = \mu I - \mu C^{-1} + \lambda(\sqrt{i_3} - 1)\sqrt{i_3}\, C^{-1} \tag{5}$$

respectively [11], [12].

[1]Here, the tissue simulations are assumed to always have errors. In low error cases (such as, for artificial data), it may be desirable to put an upper bound on the scaling factor.

In here, λ and μ are Lamé's first and second parameters, respectively, which can be calculated from Young's modulus E and Poisson's ratio ν of the material by using the relationship

$$\lambda = \frac{E\nu}{(1+\nu)(1-2\nu)} \tag{6}$$

$$\mu = \frac{E}{2(1+\nu)}. \tag{7}$$

i_n is the invariant of the right Cauchy–Green deformation tensor C where only i_1 and i_3 used here are defined as

$$i_1 = \text{trace}(C) \tag{8}$$

$$i_3 = \det(C). \tag{9}$$

IV. Simulation Based Evaluation of The Proposed Method

A. Simulation Methods

In this section, results of the simulation studies of the proposed method are presented. Several different simulation scenarios were used to validate the proposed scheme, and explore its performance under various types of uncertainties.

A limitation of *in vivo* tissue manipulation is that it is difficult to acquire the true state of the tissue to initialize computations and it has greater uncertainties compared to *ex vivo* tests.

The first simulation scenario assumed that the tissue and manipulation geometries were acquired accurately. The second scenario considered the case when the tissue geometry was not perfectly modeled. The third scenario considered the case when there were uncertainties in positioning of the end effector on the target tissue. The fourth scenario considered uncertainties in the robot's motion. And finally, the fifth scenario considered the case when the robot performs nontrivial manipulations.

In the simulations, a tissue model in the shape of a square patch, shown in Fig. 3, with dimensions of $10\,\text{cm} \times 10\,\text{cm} \times 1$ cm was used. The center of the tissue was $(0.0, 0.0, 0.0)$ in x–y–z coordinates. The end-effector gripper was assumed to grasp a 2 cm $\times$ 2 cm area on the tissue without any slip. This was modeled by anchoring the grabbed part of the tissue rigidly to the gripper by position boundary conditions. The size of the gripper was 2 cm in width and initially at $(0.04, 0.0, 0.0)$ m. The tissue was assumed to be anchored on the left side ($x = -5$ cm) and the gripper retracted the tissue by pulling in the direction of the arrow shown in Fig. 3 ($+x$-direction). The stress and strain of the tissue are assumed to be in the zero state at the beginning of the experiment including the effect of gravity.

The `Salmon` [12] open source finite element modeling and simulation package was used as the underlying FEM simulation engine, after custom modifications. The `Salmon` package offers FEM simulation with geometric and material nonlinearities. The meshing of the geometric models to be used in the FEM simulations was done by TetGen [29].

The SQP algorithm using the quasi-Newton line search, as provided by the MATLAB's fmincon function, was used to find minimum of the objective function.

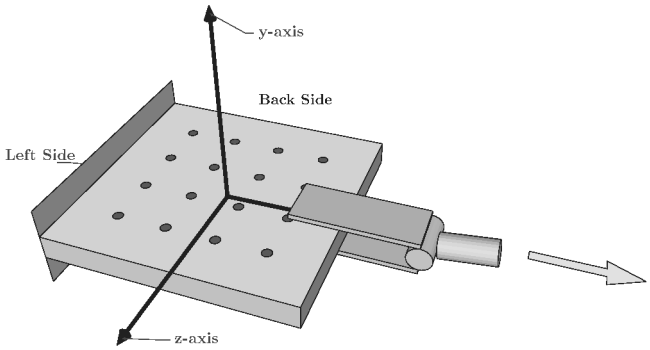

Fig. 3. Setup of the experiment shows the gripper grasping on the right side of tissue and pulling in the direction of the arrow. Sixteen fiducials apart are marked on the tissue. Spacing between rows in both direction is 20 mm.

All experiments were conducted on a 2.93 GHz Intel Core i7 CPU, and 12 GB of RAM. `Salmon` was implemented in the C++ language and MATLAB 2010b was used to implement the optimization scheme.

In the simulation scenarios, all vision and force sensing, i.e., the trajectories of the fiducials and the interaction forces were assumed to have been perfectly measured. The reference values of the sensing data were computed from simulations of a finite element model with a higher density mesh, while the estimation of the set of parameters was performed using a finite element model with a lower density mesh. Specifically, a mesh with 3122 nodes and 13473 elements was used to generate the sensing data, while a mesh with 991 nodes and 3595 elements was used in the estimation process, unless otherwise noted. The reference parameters were 15 kPa and 0.49 for Young's modulus and Poisson's ratio, respectively.

B. Simulation Results

1) Accurate Tissue and Manipulation Geometry Acquisitions: The first set of simulation studies were conducted to validate if the proposed algorithm could accurately identify the tissue parameters under ideal conditions, specifically, when perfect information about the geometry of the specimen and the geometry of manipulation (i.e., motion of the end effector relative to the target tissue) was available. The effect of the density of the finite element model mesh used in the estimation algorithm on the accuracy of the parameter estimation was also evaluated.

In case 1, the tissue model in the estimator was discretized using the higher density mesh (same as the reference). In case 2, the tissue model in the estimator was discretized using the lower density mesh.

The results in Table I show that the proposed method can accurately estimate the tissue parameters under low uncertainty conditions, and the accuracy of the method does not depend heavily on the mesh density (at least, at the range considered here).[2] The parameters estimated in case 2 were reasonably close to the actual values while the complexity is tremendously lower. Therefore, in the subsequent studies (Section IV-B2–IV-B5), the low density mesh was used in estimation while the high-density mesh was used to generate the simulated measurement data.

[2]The nonzero error value in case 1 is due to the finite tolerance value used in numerical minimization.

TABLE I
ESTIMATION RESULTS WHEN ACCURATE TISSUE AND MANIPULATION GEOMETRY MEASUREMENTS ARE AVAILABLE

Case	Case 1	Case 2
Young's Modulus (kPa)	15.18	14.98
Poisson's Ratio	0.4897	0.4849
Iterations (Function Counts)	9(30)	15(46)
Time (s) (prescaling+min)	2452(1469+983)	773 (450+90)
RMSE of		
the fiducial's position (m)	4.32e-6	8.30e-5
the force profile (N)	6.73e-5	2.37e-3

The computation time is represented as total time, which is the sum of the time for prescaling (3), and time for the actual minimization (1). RMSE stands for root mean square error.

TABLE II
EVALUATIONS OF THE METHOD AT DIFFERENT FRACTAL SCALE LEVELS

Fractal Max Height Scale	2%	4%	8%
Young's Modulus (kPa)	17.00	19.40	23.97
Poisson's Ratio	0.4693	0.4654	0.4607
Iter. (Func. Counts)	11(34)	14(42)	4(12)
Time (s) (prescaling+min)	375 (227+148)	897(729+168)	956(785+171)
RMSE of			
the fiducial's position (m)	1.15e-4	1.25e-4	1.36e-4
the force profile (N)	1.69e-3	1.85e-3	2.17e-3

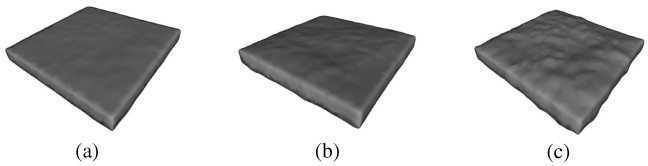

Fig. 4. Unknown parameter tissue with rough surface generated using the ridged multifractal terrain algorithm [30]. (a) Fractal maximum height scale of 2% of the tissue's original thickness. (b) Fractal maximum height scale of 4% of the tissue's original thickness. (c) Fractal maximum height scale of 8% of the tissue's original thickness.

2) Uncertainties in Tissue Geometry: The second set of simulations was conducted to evaluate the effectiveness of the method when the tissue geometry was not perfectly modeled. This was evaluated by using reference meshes which were perturbed from the original shape, while using the original mesh with the smooth surface in the estimation algorithm. The high density mesh was used to generate the test data while the low density mesh (described earlier) was used in parameter estimation.

The rough surfaces in this study were generated using the ridged multifractal terrain algorithm [30] in MeshLab [31] to represent uncertainties in tissue geometry. The results reported in Table II shows the sensitivity of the scheme to the size of the perturbations, at varying 2%, 4%, and 8% of the tissue's original thickness, as can be seen in Fig. 4.

The results demonstrated that the proposed algorithm still handled the problem quite well. Only the Young's modulus was estimated by the method was slightly off when the fractal was higher.

The algorithm that was used to generate fractal in the experiment also grew the tissue. That is the reason why Young's modulus estimated from the scheme increased as the perturbation

TABLE III
EVALUATIONS OF THE SCHEME AT ASSUMING INCORRECT GRASPING POINTS

Standard Deviation	5 mm	10 mm	20 mm
Young's Modulus (kPa)	13.82 ± 12%	12.06 ± 27%	13.33 ± 62%
Poisson's Ratio	0.4677 ± 4%	0.4574 ± 9%	0.3960 ± 28%
Time (s)	966 ± 27%	1445 ± 79%	1023 ± 60%
RMSE of			
the fiducial's position (m)	6.22e-4 ± 65%	1.71e-3 ± 79%	2.94e-3 ± 76%
the force profile (N)	4.22e-2 ± 63%	1.48e-1 ± 63%	1.63e-1 ± 107%

The parameters and other values are the results from 20 random experiments.

TABLE IV
RESULTS WHEN THE GRIPPER POSITION CONTROL SIGNAL WAS CORRUPTED WITH DIFFERENT NOISE LEVELS

Standard Deviation	10%	25%	50%
Young's Modulus (kPa)	14.65 ± 2%	13.88 ± 8%	13.41 ± 19%
Poisson's Ratio	0.4852 ± 2%	0.4733 ± 6%	0.4508 ± 13%
Time (s)	1174 ± 23%	1510 ± 36%	1190 ± 45%
RMSE of			
the fiducial's position (m)	4.14e-4 ± 30%	1.01e-3 ± 29%	2.42e-3 ± 37%
the force profile (N)	3.05e-2 ± 44%	7.66e-2 ± 34%	1.83e-1 ± 66%

The parameters and other values are the results from 20 random experiments.

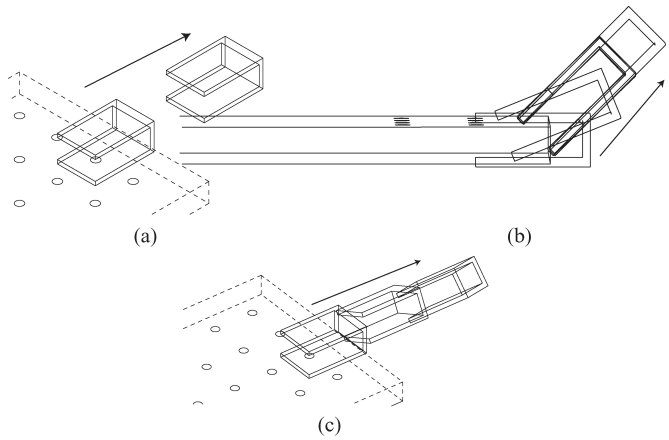

Fig. 5. Different types of complex end-effector motion used to evaluate the parameter estimation in Section IV-B5. (a) "Pull." (b) "Gradual Tangent Pull." (c) "Twist and Pull."

level increased. It is difficult to model the tissue geometry perfectly in simulation; however, the algorithm is robust to small variation shown earlier.

3) Uncertainties in the Position of the Robot's Target: The third set of simulations was conducted to evaluate the effectiveness of the method when there were uncertainties in the positioning of the end effector on the target tissue.

The simulations were done by randomly changing the center of the robot's target (the grasping point) with standard deviation of 5, 10, and 20 mm (see Table III).

The algorithm results are acceptable as shown here.

4) Uncertainties from the Robot's Motion: This set of simulations was conducted to evaluate the effectiveness of the method when there were uncertainties in robot motions. The additive Gaussian noise was generated to study the effect of uncertainties at 10%, 20%, and 50% noise levels (standard deviation of the Gaussian noise as a percent of the magnitude of the position control signal). The results are shown in Table IV.

TABLE V
PARAMETER ESTIMATION UNDER COMPLEX MOTIONS

Motion Types	"Gradual Tangent Pull"	"Twist and Pull'
Young's Modulus (kPa)	15.09	15.06
Poisson's Ratio	0.4720	0.4762
Time (s)	3057(2215+843)	1604(1014+590)
Iter. (Func. Counts)	8(29)	17(51)
RMSE of		
the fiducial's position (m)	2.17e-4	1.68e-4
the force profile (N)	2.06e-2	9.99e-3

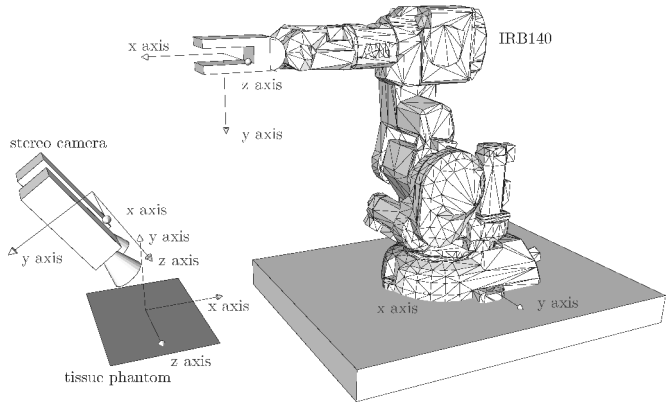

Fig. 6. Setup of the experiments with the ABB IRB 140.

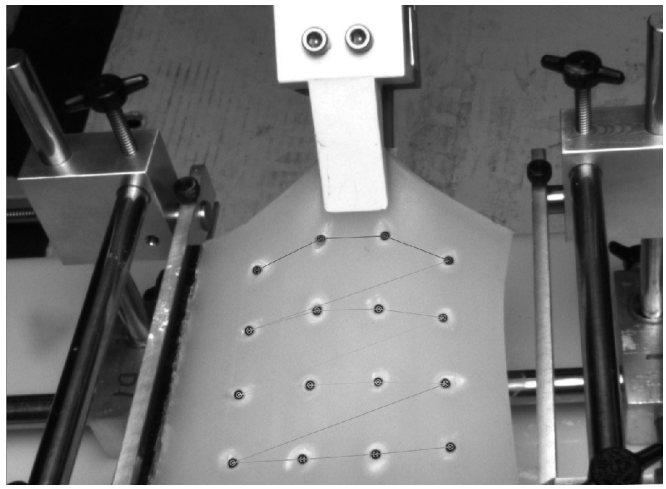

Fig. 7. Robot performing "Gradual Tangent Pull" to retract the Ecoflex 0030 tissue with mixture ratio 1:1:2 anchored two adjacent sides (on the left and at the bottom from the figure) as seen from the right camera.

Noise from the control signal appears not to cause a significant effect on the parameter estimation if the noise level is not extremely high.

5) Parameter Estimation Under Complex Motions: The merit of this multiaxial estimation framework over uniaxial estimation is the ability to estimate the tissue parameters under

TABLE VI
PARAMETER VALUES ESTIMATED BY PERFORMING DIFFERENT ROBOT MANIPULATIONS FOR DIFFERENT TISSUE PHANTOM MATERIALS WHEN ONE SIDE OF THE PHANTOM ARE CONSTRAINED

Motion Types	Pull			Gradual Tangent Pull			Twist and Pull		
Material Types (A:B:T)	1:1:0	1:1:1	1:1:2	1:1:0	1:1:1	1:1:2	1:1:0	1:1:1	1:1:2
Young's Modulus (Pa)	26450	10090	3860	26360	10310	4000	27060	10570	3870
Poisson's Ratio	0.304	0.3134	0.1683	0.2787	0.3394	0.3725	0.3465	0.3504	0.18112
Time (s) (prescaling+min)	892	418	570	1230	683	1174	804	348	2441
Iter. (Func. Counts)	11(36)	9(27)	4(21)	9(27)	9(28)	9(33)	4(12)	8(24)	14(179)

TABLE VII
PARAMETER VALUES ESTIMATED BY PERFORMING DIFFERENT ROBOT MANIPULATIONS FOR DIFFERENT TISSUE PHANTOM MATERIALS WHEN TWO ADJACENT SIDES OF THE PHANTOM ARE CONSTRAINED

Motion Types	Pull			Gradual Tangent Pull			Twist and Pull		
Material Types (A:B:T)	1:1:0	1:1:1	1:1:2	1:1:0	1:1:1	1:1:2	1:1:0	1:1:1	1:1:2
Young's Modulus (Pa)	25230	8620	4070	25250	7770	4130	24960	8660	4480
Poisson's Ratio	0.3984	0.3324	0.3984	0.3416	0.3026	0.3793	0.4157	0.2602	0.1608
Time (s) (prescaling+min)	728	1100	421	1514	1804	988	969	1840	654
Iter. (Func. Counts)	10(35)	9(27)	10(45)	20(76)	8(24)	9(30)	9(29)	25(202)	9(74)

complex surgical manipulations. This set of simulations was conducted to evaluate the effectiveness of the method when the robot had nontrivial motions during a surgical manipulation. Fig. 5 shows the two more different motions used in the simulations. In the first test motion, the gripper horizontally pulled the tissue by simultaneously rotating the gripper. And in the second case, the gripper pulled the tissue horizontally in the tissue plane while rotating the tissue to twist it.

The results in Table V show that the method can still estimate the parameters with good accuracy under such complex motions.

V. EXPERIMENTAL VALIDATION OF THE PROPOSED METHOD

A. Experimental Method

In order to validate the proposed method, hardware experiments were conducted. In the experiments, we used a soft tissue phantom created using Ecoflex 0030, a two-part silicone rubber with Silicone Thinner (nonreactive silicone fluid), from Smooth–On Inc., which was used in [32]. The silicone phantoms with three different consistencies of Silicone Thinner were used in order to cover a wide range of parameter values. ABB IRB 140, a 6-DOF robot equipped with the Gamma SI-130-10 force sensor (ATI Industrial Automation, Inc., Apex, NC) with resolution of 1/20 N was used to collect the manipulation trajectories and force sensing data. The repeatability of the robot is 0.03 mm. The setup of the experiments is shown in Fig. 6.

The tissue phantoms used in the experiments were similar in shape and size to the models used in the simulation studies described in Section IV-A. Specifically, the tissue phantoms were square in shape, with dimensions of $10\,\text{cm} \times 10\,\text{cm} \times 1\,\text{cm}$. The tissue phantoms were placed horizontally while being grabbed and retracted by a gripper toward right. We considered two cases where the phantoms were anchored to a wall on one side (left) and two adjacent sides (left and back). The retraction actions were achieved by moving the gripper in 1–2 mm increments, toward right, producing about 10% elongation of the tissue phantom as shown in Fig. 5. The "Pull" trajectory was performed in 10 steps with 2 mm increments; the "Gradual Tangent Pull" trajectory was performed in 20 steps with $\sim$1 mm increments; and the "Twist and Pull" trajectory was performed in 10 steps with $\sim$2 mm increments. Sixteen artificial fiducials were marked on the top surface of the tissue and were tracked by a calibrated stereo camera pair to measure their deformations during retraction.

The silicone surface was labeled with rubber beads 1 mm in diameter which were used as the fiducials. The stereo vision system employed two of identical FL2G-13S2C 1.2MP cameras (Point Gray Research, Richmond, BC, Canada). The cameras were placed at a distance of 30 cm. The cameras were programmed using the Flycapture library (Point Gray Research, Richmond, BC, Canada) and OpenCV. Once the fiducials were detected, each individual fiducial location was calculated by distinguishing each fiducial in the image. After the fiducials were detected in the stereo image pair (see Fig. 7), the actual locations of the fiducials were triangulated using the camera calibration information.

One important concern regarding experimental validation of the proposed methods is the availability of baseline material parameters (Young's modulus and Poisson's ratio) for the silicone rubber used in constructing the phantoms. The only material property that the authors could identify in the literature for Ecoflex 0030 was for the 1:1:0 mixture proportions [32].[3] Hollenstein has reported a Young's modulus of 29.5 kPa, while a Poission ratio of 0.5 was assumed. In order

[3]To the best of our effort, these were the only parameter values that we were able to find in the literature for the Ecoflex silicone.

TABLE VIII

ACTUAL (SHOWN IN SOLID) AND THE PREDICTED (SHOWN IN DASH) INTERACTION FORCE PROFILES IN TISSUE COORDINATE FRAME (X-, Y-, AND Z-AXES ARE SHOWN IN BLUE, GREEN, AND RED, RESPECTIVELY) AND THE ACTUAL (BLACK/DARK) AND PREDICTED (RED/BRIGHT) TRAJECTORIES OF THE FIDUCIAL MARKERS WHEN TWO ADJACENT SIDES OF THE PHANTOM ARE CONSTRAINED

Ecoflex 0030 Mixing Ratio		
1:1:0	1:1:1	1:1:2
Pull		
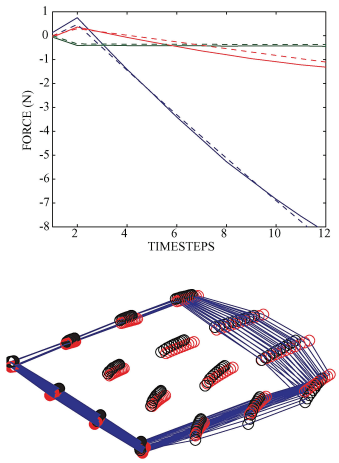	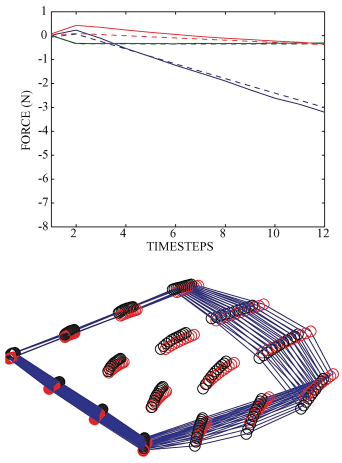	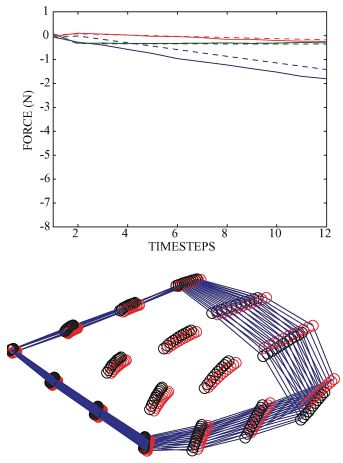
Gradual Tangent Pull		
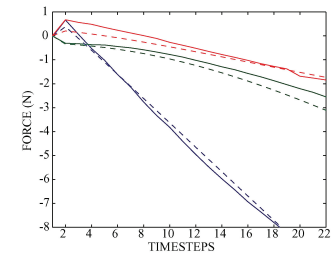	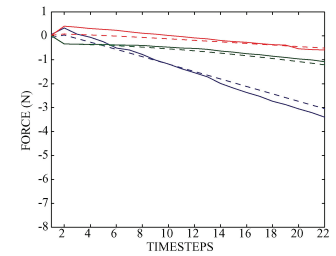	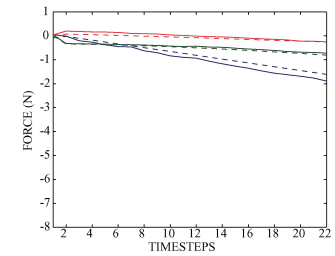
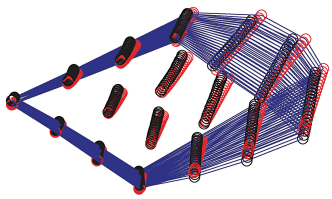	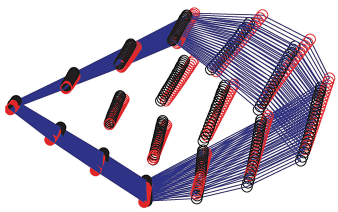	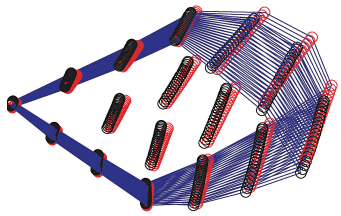
Twist and Pull		
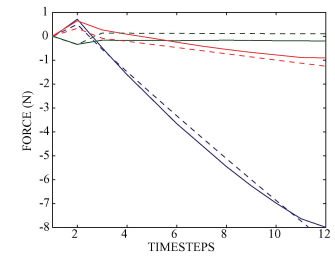	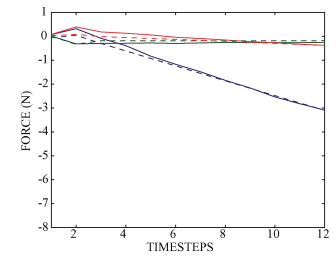	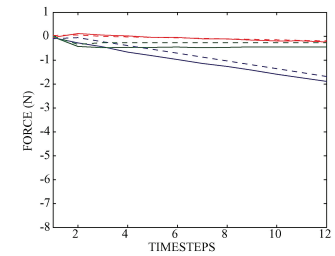
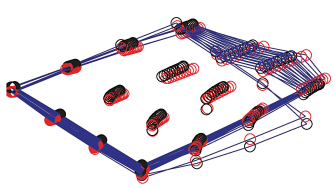	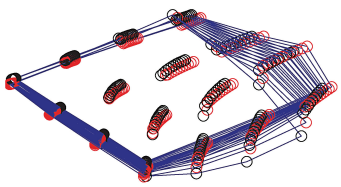	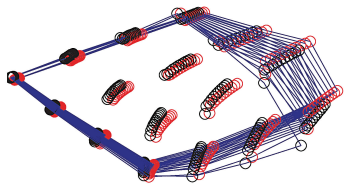

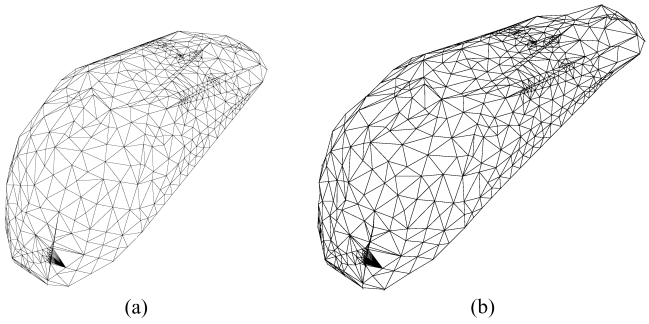

Fig. 8. (a) Undeformed and (b) deformed liver models. The model was anchored on the left side while being grasped and pulled on the right side.

to obtain the necessary baseline material property data, we conducted standard uniaxial loading tests. Specifically, hourglass-shaped specimens of the silicone rubber material were constructed and they were tested on a universal testing machine (Instron 1026). Young's moduli estimated by the uniaxial testing of Ecoflex 0030 for the mixture proportions 1:1:0, 1:1:1, and 1:1:2 were, respectively, 36.21 ± 2.62 kPa, 10.91 ± 1.54 kPa, and 5.29 ± 1.92 kPa. A Poisson's ratio of 0.5 was assumed.

The stress and strain of the tissue are assumed to be in zero state at the beginning of the experiment. Here, we do not neglect the effect of gravity.

B. Experimental Results

Different tissue consistencies were obtained by using different silicone rubber and silicone thinner proportions during the preparation of the phantoms. The parameter estimates for the three different tissue phantoms are reported in Tables VI and VII. The values estimated here using the proposed method are very close to the reported parameter values for the Ecoflex 0030 mixture ratio of 1:1:0 from the literature [32] and the results from the universal testing machine for the mixture ratio of 1:1:1 and 1:1:2 in Section V-A. Note that, using the proposed method, we estimated both Young's moduli and Poisson's ratios simultaneously instead of assuming Poisson's ratios to be 0.5. Estimating the parameters simultaneously helps us to have a better prediction in geometric configurations of the tissue.

In order to save space, the figures showing the trajectories of the fiducials and the force profiles for the cases in Table VI are omitted. The trajectories of fiducials and the force profiles for the cases in Table VII are shown in Table VIII. The figures in Table VIII show that the fiducial trajectories and force profiles start to deviate from the actual trajectories for large deformations, even though there is a good agreement between the estimated and actual trajectories for relatively smaller deformations. Note that in constrast to some literatures (for example [32]), Poisson's ratio was actually estimated from the algorithm instead of assuming the value to 0.5. Doing this way, we found that the estimated tissue responses and the real physical data are in a better agreement than the response assuming Poisson's ratio to such a number. We believe this deviations are due to the material type used, as Neo–Hookean might not be the best choice for highly nonlinear materials.

VI. Example: Parameter Estimation With More Complex Object Geometries

The parameter estimation examples presented earlier in this paper primarily used regular shapes for object geometry in order to allow easier interpretation of the results. The proposed method is also applicable to more complex object shape, such as those that would be encountered in practical applications.

In order to evaluate the performance of the proposed method for nonregular object geometries, a simulation study was conducted. In this simulation, a tissue model in the shape of liver, shown in Fig. 8(a), was used [33]. The liver model was assumed to be anchored on one side while being grasped and pulled on the opposite side, as shown in Fig. 8(b). The reference deformation and force trajectories were generated using a 2803 node and 13737 element mesh model, using Young's modulus value of 15 kPa and Poisson's ratio of 0.35. The parameter estimation was performed using a 1033 node and 4095 element mesh model.

The parameters estimated using the presented algorithm were 13.36 kPa and 0.30 for Young's modulus and Poisson's ratio, respectively. The mean error of fiducial trajectories estimated from the the estimated parameters was less than 0.9 mm and was less than 0.46% of the total trajectory. The maximum force error was 1.5 N and that was 2.2% of the total force. It is demonstrative that the algorithm may also be used for parameter estimation for nonregular object shapes.

VII. Discussion and Conclusion

This paper presented a new inverse nonlinear finite element-based scheme to estimate the mechanical parameters of soft tissues using data collected during regular manipulation of the tissue in robotic surgery. The method uses a hyperelastic material model for the tissue. Several challenge scenarios and different types of complex motions were considered to test the sensitivity of the proposed scheme. Results of the method are evaluated and validated experimentally as well. The simulation and experimental results indicated that the proposed scheme is effective in estimating the parameters in general.

Typical surgical manipulation motions are relatively slow. Therefore, the tissue deformations and interactions forces were approximated as quasi-static, ignoring the viscous and inertial effects.

It is important to note that the proposed approach assumed homogeneous material. Although the proposed approach could be applicable for moderate nonhomogeneities, the identification of a very detailed inhomogeneous model (e.g., objects with lots of embedded fine structures), where identifications of the material parameters of the embedded fine structures are sought, would require a more data-rich method, such as magnetic resonance elastography [25], [34]–[37] and ultrasound elastometry [38].

Uncertainty in boundary conditions, including complex boundary conditions, such as frictional sliding contact resulting from an object sliding over another object, has been considered

in this study to some extent. The aspect of the problem needs to be further studied.

It is also important to note that the choice of the Neo–Hookean material type is not fundamental to the proposed method. The same overall tissue parameter estimation method can also be applied by using different underlying material types. However, whether the sufficient accuracy is obtainable or not for different material types needs to be verified. A detailed analysis and comparison of different material types is outside the scope of this paper.

ACKNOWLEDGMENT

The authors would like to thank Prof. J. Lewandowski and Prof. W. Newman for their valuable suggestions and for allowing us to use the facilities to perform the experiments. They would also like thank R. Jackson and C. Balin for their stereo-vision implementations.

REFERENCES

[1] P. Boonvisut, R. Jackson, and M. C. Çavuşoğlu, "Estimation of soft tissue mechanical parameters from robotic manipulation data," in *Proc. Int. Conf. Robot. Autom.*, May 2012, pp. 4667–4674.

[2] S. Hirai, T. Tsuboi, and T. Wada, "Robust grasping manipulation of deformable objects," in *Proc. IEEE Int. Symp. Assembly Task Planning*, 2001, pp. 411–416.

[3] K. Gopalakrishnan and K. Goldberg, "D-Space and deform closure grasps of deformable parts," *Int. J. Robot. Res.*, vol. 24, no. 11, pp. 899–910, 2005.

[4] M. Moll and L. E. Kavraki, "Path planning for deformable linear objects," *IEEE Trans. Robot.*, vol. 22, no. 4, pp. 625–636, Aug. 2006.

[5] M. Saha and P. Isto, "Motion planning for robotic manipulation of deformable linear objects," in *Proc. IEEE Int. Conf. Robot. Autom.*, 2006, pp. 2478–2484.

[6] M. Saha and P. Isto, "Manipulation planning for deformable linear objects," *IEEE Trans. Robot.*, vol. 23, no. 6, pp. 1141–1150, Dec. 2007.

[7] R. Alterovitz, M. Branicky, and K. Goldberg, "Motion planning under uncertainty for image-guided medical needle steering," *Int. J. Robot. Res.*, vol. 27, no. 11–12, pp. 1361–1374, Nov. 2008.

[8] R. Alterovitz, K. Y. Goldberg, J. Pouliot, and I. C. Hsu, "Sensorless motion planning for medical needle insertion in deformable tissues," *IEEE Trans. Inf. Technol. Biomed.*, vol. 13, no. 2, pp. 217–225, Mar. 2009.

[9] R. Jansen, K. Hauser, N. Chentanez, F. van der Stappen, and K. Goldberg, "Surgical retraction of non-uniform deformable layers of tissue: 2D robot grasping and path planning," in *Proc. IEEE Int. Conf. Intell. Robots Syst.*, St Louis, MO, Oct. 2009, pp. 4092–4097.

[10] M. Bro-nielsen, "Finite element modeling in surgery simulation," *Proc. IEEE: Special Issue on Surgery Simulation*, vol. 86, pp. 490–503, 1998.

[11] X. Wu, "Design of an interactive nonlinear finite element based deformable object simulator," Ph.D. dissertation, Dept. Mech. Eng., Univ. California Berkeley, Berkeley, 2002.

[12] H.-W. Nienhuys, "Cutting in deformable objects," Ph.D. dissertation, Inst. Inf. Comput. Sci., Utrecht Univ., Utrecht, The Netherlands, 2003.

[13] M. Müller, J. Dorsey, L. McMillan, R. Jagnow, and B. Cutler, *Stable Real-Time deformations.* New York: ACM Press, 2002, pp. 49–54.

[14] J. Barbič and D. L. James, "Real-time subspace integration for St. Venant-Kirchhoff deformable models," *ACM Trans. Graph. (SIGGRAPH)*, vol. 24, no. 3, pp. 982–990, Aug. 2005.

[15] D. R. Veronda and R. A. Westmann, "Mechanical characterization of skin—Finite deformations," *J. Biomech.*, vol. 3, no. 1, pp. 111–124, Jan. 1970.

[16] H. Mehrabian and A. Samani, "Constrained hyperelastic parameters reconstruction of PVA (Polyvinyl Alcohol) phantom undergoing large deformation," in *Medical Imaging 2009: Visualization, Image-Guided Procedures, and Modeling*, M. I. Miga and K. H. Wong, Eds., vol. 7261. Bellingham, WA: SPIE, 2009, no. 1.

[17] K. Sangpradit, H. Liu, L. D. Seneviratne, and K. Althoefer, "Tissue identification using inverse finite element analysis of rolling indentation," in *Proc. IEEE Int. Conf. Robot. Autom.*, May 2009, pp. 1250–1255.

[18] M. P. Ottensmeyer, "Minimally invasive instrument for *in vivo* measurement of solid organ mechanical impedance," Ph.D. dissertation, Dept. Mech. Eng., Massachusetts Inst. Technol., Cambridge, MA, 2001.

[19] M. Kauer, V. Vuskovic, J. Dual, G. Szekely, and M. Bajka, "Inverse finite element characterization of soft tissues," *Med. Image Anal.*, vol. 6, no. 3, pp. 275–287, 2002.

[20] I. Brouwer, J. Ustin, L. Bentley, A. Sherman, N. Dhruv, and F. Tendick, "Measuring *in vivo* animal soft tissue properties for haptic modeling in surgical simulation," *Stud. Health Technol. Inf.*, vol. 81, pp. 69–74, 2001.

[21] J. Lang, D. K. Pai, and R. J. Woodham, "Acquisition of elastic models for interactive simulation," *Int. J. Robot. Res.*, vol. 21, no. 8, pp. 713–733, Aug. 2002.

[22] B. Bickel, M. Bächer, M. A. Otaduy, W. Matusik, H. Pfister, and M. Gross, "Capture and modeling of non-linear heterogeneous soft tissue," in *Proc. ACM SIGGRAPH*, 2009, pp. 1–9.

[23] P. Fong, "Sensing, acquisition, and interactive playback of data-based models for elastic deformable objects," *Int. J. Robot. Res.*, vol. 28, no. 5, pp. 630–655, May 2009.

[24] B. Frank, R. Schmedding, C. Stachniss, M. Teschner, and W. Burgard. (2010, Oct.). "Learning the elasticity parameters of deformable objects with a manipulation robot," pp. 1877–1883, [Online]. Available: http://dx.doi.org/10.1109/IROS.2010.5653949

[25] A. E. Kerdok, S. M. Cotin, M. P. Ottensmeyer, A. M. Galea, R. D. Howe, and S. L. Dawson, "Truth cube: Establishing physical standards for soft tissue simulation," *Med. Image Anal.*, vol. 7, no. 3, pp. 283–291, Sep. 2003.

[26] Z. Gao, K. Lister, and J. Desai, "Constitutive modeling of liver tissue: Experiment and theory," *Ann. Biomed. Eng.*, vol. 38, no. 2, pp. 505–516, 2010.

[27] D. d'Aulignac, M. C. Çavuşoglu, and C. Laugier, "Modeling the dynamics of the human thigh for a realistic echographic simulator with force feedback," in *MICCAI '99: Proceedings of the Second International Conference on Medical Image Computing and Computer-Assisted Intervention*. London, U.K.: Springer-Verlag, 1999, pp. 1191–1198.

[28] G. Irving, J. Teran, and R. Fedkiw, "Invertible finite elements for robust simulation of large deformation," in *SCA '04: Proceedings of the 2004 ACM SIGGRAPH/Eurographics Symposium on Computer Animation*. Aire-la-Ville, Switzerland: Eurographics Association, 2004, pp. 131–140.

[29] H. Si, "Tetgen: A quality tetrahedral mesh generator and a 3D delaunay triangulator," [Online]. Available: http://tetgen.berlios.de/.

[30] D. S. Ebert, F. K. Musgrave, D. Peachey, K. Perlin, and S. Worley, *Texturing and Modeling, Third Edition: A Procedural Approach (The Morgan Kaufmann Series in Computer Graphics)*, 3rd ed. San Mateo, CA: Morgan Kaufmann, Dec. 2002.

[31] P. Cignoni, M. Callieri, M. Corsini, M. Dellepiane, F. Ganovelli, and G. Ranzuglia. (2008). "MeshLab: An Open-Source mesh processing tool," pp. 129–136, [Online]. Available: http://vcg.isti.cnr.it/Publications/2008/CCCDGR08

[32] M. Hollenstein, "Mechanical characterization of soft materials: Comparison between different experiments on synthetic specimens," Master's thesis, Inst. Mech. Syst. Dept. Mech. Process Eng., ETH Zurich, Eidgenössische Technische Hochschule Zurich, Zurich, Switzerland, 2008.

[33] J. Allard, S. Cotin, F. Faure, P.-J. J. Bensoussan, F. Poyer, C. Duriez, H. Delingette, and L. Grisoni, "SOFA—An open source framework for medical simulation," *Stud. Health Technol. Informat.*, vol. 125, pp. 13–18, 2007.

[34] X. Shi, R. W. Martin, D. Rouseff, S. Vaezy, and L. A. Crum, "Detection of high-intensity focused ultrasound liver lesions using dynamic elastometry," *Ultrason. Imag.*, vol. 21, no. 2, pp. 107–126, Apr. 1999.

[35] R. Sinkus, J. Lorenzen, D. Schrader, M. Lorenzen, M. Dargatz, and D. Holz, "High-resolution tensor MR elastography for breast tumour detection," *Phys. Med. Biol.*, vol. 45, no. 6, pp. 1649–1664, Jun. 2000.

[36] S. K. Venkatesh, M. Yin, J. F. Glockner, N. Takahashi, P. A. Araoz, J. A. Talwalkar, and R. L. Ehman, "MR elastography of liver tumors: Preliminary results," *AJR. Amer. J. Roentgenol*, vol. 190, no. 6, pp. 1534–1540.

[37] S. F. Bensamoun, L. Wang, L. Robert, F. Charleux, J.-P. P. Latrive, and M.-C. Ho Ba Tho, "Measurement of liver stiffness with two imaging techniques: Magnetic resonance elastography and ultrasound elastometry," *J. Magn. Reson. Imag.*, vol. 28, no. 5, pp. 1287–1292, Nov. 2008.

[38] E. Turgay, S. Salcudean, and R. Rohling, "Identifying the mechanical properties of tissue by ultrasound strain imaging," *Ultrasound Med. Biol.*, vol. 32, no. 2, pp. 221–235, Feb. 2006.

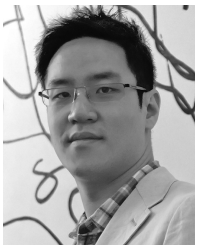

Pasu Boonvisut (S'12) received the B.Eng. and M.Eng. degrees in electrical engineering from Chulalongkorn University, Bangkok, Thailand, in 2005 and 2007, respectively. He is currently working toward the Ph.D. degree at Case Western Reserve University, Cleveland, OH.

His research interests include medical robotics and digital signal processing.

M. Cenk Çavuşoğlu (S'93–M'01–SM'06) received the B.S. degree in electrical and electronic engineering from Middle East Technical University, Ankara, Turkey, in 1995, and the M.S. and Ph.D. degrees in electrical engineering and computer sciences from the University of California, Berkeley, in 1997 and 2000, respectively.

He is currently an Associate Professor of electrical engineering and computer science at Case Western Reserve University, Cleveland, OH. Previously, he was a Visiting Researcher at the INRIA Rhones-Alpes Research Center, France, in 1998, a Postdoctoral Researcher and Lecturer at the University of California, Berkeley, from 2000 to 2002, and a Visiting Associate Professor at Bilkent University, Ankara, Turkey, from 2009 to 2010. His research involves applications of robotics and control engineering to biomedical and biologically inspired engineered systems. Specifically, his research interests include robotics, systems and control theory, and human–machine interfaces, with emphasis on medical robotics, haptics, virtual environments, surgical simulation, and biosystem modeling and simulation.

Dr. Çavuşoğlu is currently serving as an Associate Editor of the IEEE TRANSACTIONS ON ROBOTICS, and as a Technical Editor of the IEEE/ASME TRANSACTIONS ON MECHATRONICS.